To the Graduate Council:

I am submitting herewith a thesis written by Matthew Stuart McElhaney entitled "Petrogenesis of the Chunky Gal Mountain Mafic-Ultramafic Complex." I have examined the final copy of this thesis for form and content and recommend that it be accepted in partial fulfillment of the requirements for the degree of Master of Science, with a major in Geology.

Harry Y. McSween, Jr.
Major Professor

We have read this thesis and recommend its acceptance:

Fred B. Keller

Karla C. Mimra

Accepted for the Council:

L. Evans Haith
Vice Chancellor
Graduate Studies and Research

PETROGENESIS OF THE CHUNKY GAL MOUNTAIN MAFIC-ULTRAMAFIC COMPLEX

A Thesis

Presented for the

Master of Science

Degree

The University of Tennessee, Knoxville

Matthew Stuart McElhaney

December 1981

ACKNOWLEDGMENTS

The author would like to thank committee chairman, Dr. Harry Y. McSween, Jr., for suggesting the topic of this study, and for his continued guidance and encouragement throughout the project. Discussions with committee members, Dr. Fred B. Keller and Dr. Kula C. Misra, regarding alpine-type ultramafic bodies in the southern Appalachian Blue Ridge, and their help in preparing the final draft are greatly appreciated. Dr. Keller provided valuable insight into the nature and scope of tectonic problems encountered in the southern Appalachians. Discussions with Dr. Robert H. Hunter concerning X-ray fluorescence correction procedures and data interpretation also proved helpful.

The author would also like to acknowledge Mr. Charles Nicks, of Buck Creek, North Carolina, for access to his land and the gracious loan of his private collection of literature on the mining activity and geological investigations in the Buck Creek area. The U.S. Forest Service allowed access to lands under their jurisdiction and gave permission to the author to camp and collect samples in politically sensitive areas.

Financial assistance was provided by grants from Sigma Xi and from The University of Tennessee, Knoxville, Geology Department Professor's Honors Fund (through a donation by Gilbert H. Boyd). EG&G ORTEC, in Oak Ridge, graciously provided access to their X-ray fluorescence lab, where all bulk chemical analyses were performed.

Final thanks go to my wife, Sharla, for typing drafts, and most of all for helping to keep this whole project in proper perspective.

ABSTRACT

The Buck Creek ultramafic body lies within a fairly continuous belt of alpine-type ultramafics in the North Carolina Blue Ridge. This body is completely enveloped by the Chunky Gal Mountain amphibolites. This paper explores possible relationships between these two lithologic units. Structural relationships indicate that at least three periods of deformation affected the entire complex. Cataclasis along portions of the mafic-ultramafic contact, and a thrust contact between the amphibolite and the surrounding Carolina Gneiss, indicate a tectonic mode of emplacement for all lithologies within the complex. The amphibolites are divided into two units, Type I and Type II, on the basis of texture, mineralogy, trace element chemistry, and geothermometry. Type I amphibolites were metamorphosed under prograde granulite facies conditions (~750°C) and oxygen fugacities approximate to the HM buffer, while Type II amphibolites were metamorphosed under prograde amphibolite facies conditions (~510°C) and oxygen fugacities approximate to the QFM buffer. Pressure was approximately 4-6 kb over the entire complex. A second, retrograde event was of lower greenschist facies. The amphibolites appear to have been derived from a cumulate gabbroic protolith, and many igneous differentiation trends are preserved despite the high grades of metamorphism. This complex may represent the basal section of an ophiolite sequence or a rifted continental mafic pluton into which an ultramafic diapir has intruded.

TABLE OF CONTENTS

LIST OF TABLES

LIST OF FIGURES

FIGURE PAGE

LIST OF PLATES

PLATE

CHAPTER I

INTRODUCTION

Statement of the Problem

The Buck Creek ultramafic body, in northeastern Clay County, North Carolina (Figure 1), lies within a fairly continuous belt of ultramafic rocks in the eastern Blue Ridge province of the southern Appalachians. The origin and mode of emplacement of these alpine-type ultramafic bodies have long been enigmatic. As of yet, none of the proposed models for their genesis has adequately explained all of the features observed in the ultramafic occurrences of this region. Only a few current tectonic models have attempted to integrate the occurrence of Blue Ridge ultramafics with the geodynamic evolution of the Appalachian orogen (Chidester and Cady, 1972; Stevens et al., 1974; Rankin, 1975; Hatcher, 1978; Misra and Keller, 1978).

Two vastly different explanations for the origin of ultramafic bodies in the Blue Ridge have been reviewed by Misra and Keller (1978):

1. The ultramafic bodies represent dismembered ophiolite fragments or ophiolitic mélange;
2. The ultramafic bodies are diapiric intrusives emplaced into sedimentary and volcanic rocks of eugeosynclinal affinity.

It is clear from the above two viewpoints that significantly different models for the evolution of the southern Appalachian orogen may be

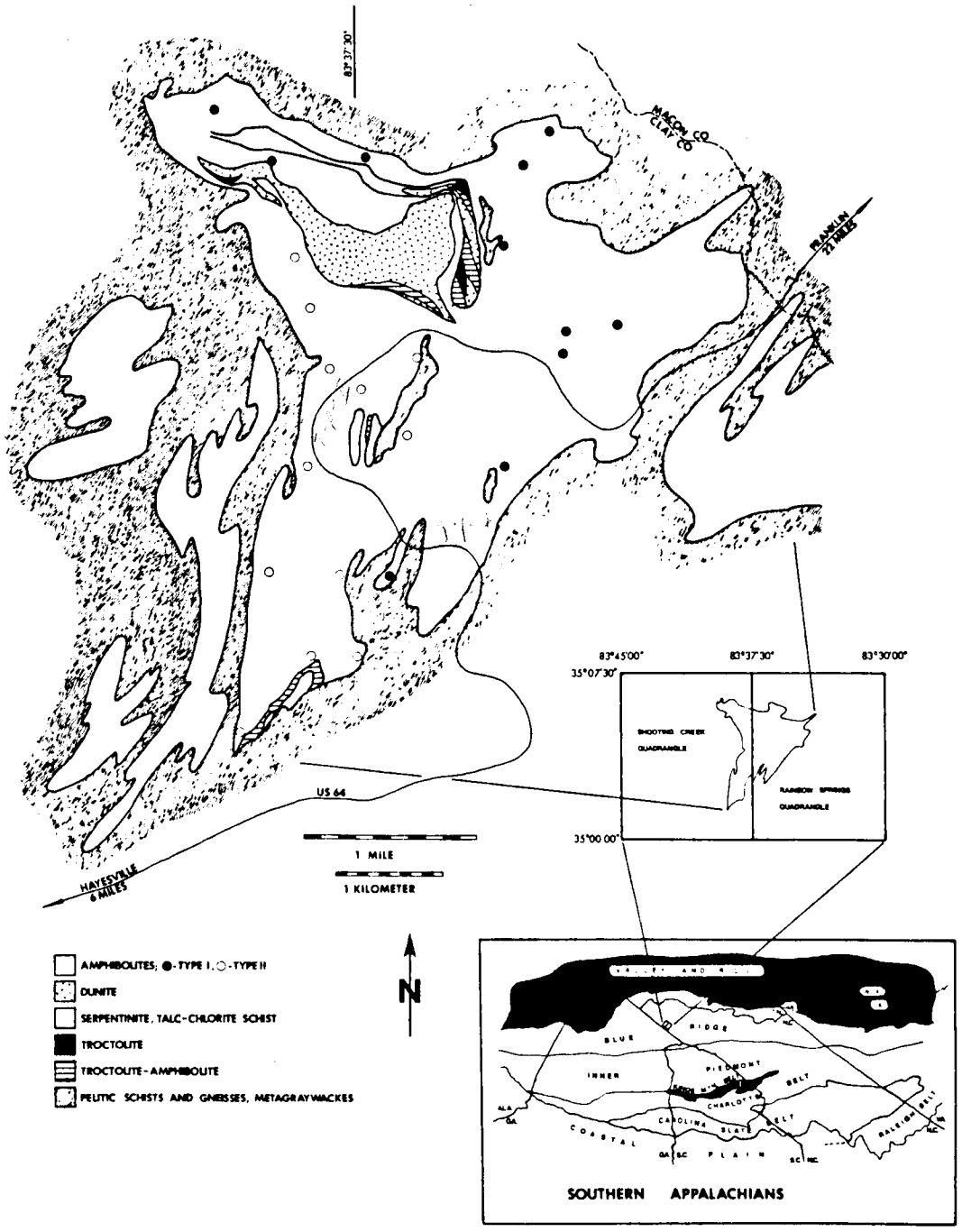

Figure 1. Lithologic map of the Chunky Gal Mountain mafic-ultramafic complex in Clay County, North Carolina, with regional inset showing the position of the complex in the eastern Blue Ridge province of the southern Appalachians. Filled circles and open circles represent chemically analyzed Type I and Type II amphibolites, respectively.

envisaged depending upon which, if either, of the above explanations is correct. However, distinguishing between these alternatives is difficult.

One important feature which some of these ultramafic bodies share is a close spatial relationship with enveloping mafic rocks, notably amphibolites (Hurst, 1973; Hartley, 1973; Petty and Hatcher, 1980; Swanson, 1980; McElhaney and McSween, 1981). These mafic rocks belong to the Roan Gneiss of Keith (1903) and have been variously interpreted as (1) metamorphosed igneous rocks intrusive into metasediments of the Carolina Gneiss (Keith, 1903), (2) para-amphibolites derived from metamorphism of impure carbonate layers within a sedimentary sequence (Parker, 1952; Brobst, 1962), or (3) metabasaltic flows or shallow intrusives interlayered with metasediments of the Carolina Gneiss (Hadley, 1970). The volcanic and clastic facies of the Ashe Formation, in the northeastern Blue Ridge of North Carolina also contain ultramafic bodies and are considered by Rankin (1970) to be equivalents of the Roan and Carolina Gneisses, respectively. To the southwest in northern Georgia, the ultramafic rocks are associated with mafic rocks of the upper Ashland (Hurst, 1955; Hurst and Jones, 1973) and metasediments of the lower Ashland (Hurst, 1973). The Ashland sequence is similar to the Ashe in the northeast and may be correlative (Hurst, 1973).

It is possible that the ultramafic rocks were tectonically emplaced into intercalated volcanic and sedimentary rocks which are unrelated to the ultramafics (e.g., Rankin et al., 1973). However, the close proximity of these amphibolites to some of the Blue Ridge ultramafic bodies suggests a possible genetic relationship (Hopkins, 1914; Hartley,

1973; Hartley and Penley, 1974; Petty and Hatcher, 1980; McElhaney and McSween, 1981). To evaluate possible petrogenetic relationships between an ultramafic body and its enclosing amphibolites, the Chunky Gal Mountain mafic-ultramafic complex (McElhaney and McSween, 1981) was investigated. This complex contains the Buck Creek ultramafic body, which has been studied previously by Hadley (1949), Kuntz (1964), and Sailor and Kuntz (1973). Structural, petrologic, and geochemical studies of the mafic rocks of the complex are the subject of this report. An understanding of the petrogenesis of the amphibolites may unravel the complex mechanism by which the associated ultramafic rocks were emplaced.

Field Methods and Analytical Techniques

Field mapping of the Chunky Gal Mountain mafic-ultramafic complex (Plate I) consisted of verifying lithologic contacts of the Buck Creek ultramafic body as shown on Hadley's (1949) and Kuntz's (1964) maps and modification of Hatcher and Butler's (1979) map of the enveloping mafic rocks. Particular emphasis was placed on determining the nature of both the ultramafic-mafic and mafic-Carolina Gneiss contacts. Due to lack of outcrop, deep soil cover, and often dense vegetation, the actual mafic ultramafic contact was not directly observed. However, the nature of this contact as described by Hadley (1949) was confirmed by the work of Kuntz (1964), as well as by three petrographic traverses completed during the present study. The mafic-gneiss contact is well exposed along highways in the southern portion of the body; elsewhere the contact

was mapped from float. Measurements of strike and dip of foliation, joints, and fold axial surfaces were collected, as well as orientations of major and minor fold hinges, slickensides, and other lineations.

Over two hundred samples of amphibolite, ultramafic lithologies, and Carolina gneisses and schists were collected in order to provide coverage of the entire complex. Thin sections were prepared from samples cut perpendicular to foliation. These thin sections, twenty-five of which were polished, were examined using both transmitted and reflected light microscopy.

Twenty-five samples of amphibolite (see Plate I for locations) were prepared for X-ray fluorescence bulk chemical analysis using techniques described by Wheeler (1979). Pressed-powder pellets were analyzed with an ORTEC TEFA III (Tube Excited X-Ray Fluorescence Analyzer) using six USGS rock standards (Flanagan, 1969, 1976) and five South African rock standards (Russell et al., 1972) and employing various run conditions for major and trace elements (Appendix A). Total iron was calculated as Fe_2O_3. Correction procedures were those described by Hasler and Kemp (1957).

Mineral analyses were performed on nine of the amphibolite samples used for XRF analysis, as well as several ultramafic and Carolina Gneiss samples, with an automated MAC 400S electron microprobe, using appropriate natural and synthetic standards. An accelerating voltage of 15 Kv was used. A beam current of 0.03 μA and a defocused beam were used in analyses of amphiboles, plagioclase, scapolite, and biotite, while a beam current of 0.05 microamps and a beam diameter of 1 μm were used to

analyze all other phases. Correction procedures were those of Bence and Albee (1968), utilizing data of Albee and Ray (1970). Where possible three to ten analyses were performed on each grain, and average values and 1 σ standard deviations were computed. Amphibole analyses were recalculated using the procedure of Leake (1978), while Fe^{2+} and Fe^{3+} in oxide phases were calculated based on cation charge and stoichiometry. Several representative amphiboles and scapolites were analyzed by Energy Dispersive methods to determine the volatile constituents present. A beam current of 0.005 μA and a counting time of sixty seconds were used.

Various statistical routines, such as cluster analysis and correlation by Spearman and Pearson coefficients, were performed on whole-rock and microprobe data (Barr et al., 1979). An attempt was made to calculate modes from bulk and mineral analyses using the program MOD II (Wright and Doherty, 1970); however, the data were not amenable to such an approach for reasons cited by Perry (1967, 1969). CIPW norms were also calculated using an assumed Fe^{2+}/Fe^{3+} ratio of 0.71. This ratio is an average derived from 215 amphibolite analyses taken from various sources (e.g., Evans and Leake, 1960; Engel and Engel, 1962; Gomes et al., 1962; Tobisch, 1968; Van de Kamp, 1969; Glassley and Sørensen, 1978; Bard and Moine, 1979), where analyses of both FeO and Fe_2O_3 were reported. No assumptions were made regarding the origin of the amphibolite, so that no bias would be introduced when choosing analyses from the literature.

CHAPTER II

FIELD AND STRUCTURAL RELATIONSHIPS

Lithologic Units and Field Relations

The Chunky Gal Mountain complex can be conveniently subdivided into the Buck Creek ultramafic unit and the mafic envelope rocks. The Buck Creek ultramafic body is located in the northwestern portion of the complex (Figure 1), and contains most of the ultramafic lithologies found within the complex. Several smaller concordant lenses of ultramafic rocks occur within the amphibolites. The complex lies within garnet-muscovite schists and biotite gneisses of the Carolina Gneiss (Keith, 1903), considered to be part of the Coweeta Group by Hatcher and Butler (1979).

The Buck Creek ultramafic body is composed primarily of dunite, which weathers more rapidly than the enveloping rocks to form topographically low areas. There is a distinct change in vegetation across the mafic-ultramafic contact, from a deciduous flora to scrub pine. All vegetation appears stunted where underlain by dunite. The dunite in several places has altered to serpentinite and talc-chlorite schist. The smaller ultramafic lenses within the complex are almost entirely serpentinized.

A small portion of the Buck Creek body is composed of coronite-troctolite, an olivine plagioclase cumulate which contains reaction rims (coronas) between olivine and plagioclase. These reaction rims

are resistant to weathering and stand out, imparting a characteristic knobby appearance to the rock. As modal olivine decreases, the coronas become smaller and are segregated into bands which form resistant ridges. In some areas of the body, the troctolite grades into anorthosite. Amphibolite derived from metamorphism of troctolite occurs with troctolite as abundant dikes within the main dunite body and as large en echelon lenses in a subsidiary body (Hadley, 1949).

Enveloping mafic rocks are composed almost exclusively of amphibolite, which is fairly resistant to weathering and stands out in marked contrast to the dunite. Outcrops are generally abundant and fresh, except in lower-lying areas where the amphibolite forms a distinctive reddish saprolite. In many cases the amphibolite is differentiated into light and dark bands from 3-15 mm in width. These bands are accentuated by selective weathering of those containing plagioclase, leaving behind ridges composed of more resistant amphibole. Another abundant type of amphibolite has no mineral segregations and a finer grain size than the banded amphibolites, imparting a characteristic "salt and pepper" appearance.

Several large pods of garnet-muscovite schist appear within the amphibolite (Figure 1, p. 2) and are thought to be infolded remnants of the surrounding Carolina Gneiss. These schists weather to an orange soil containing abundant muscovite and garnet. Several quartz-plagioclase pegmatities also occur within the amphibolite.

Carolina Gneiss-Amphibolite Contacts

The contact between the Carolina Gneiss and the amphibolite appears to be a major thrust fault which may border a large portion of the complex (Figure 2). This fault, which is well exposed along the southern portion of the body, has been mapped as the Chunky Gal Mountain thrust fault by Hatcher and Butler (1979). They also show the two smaller amphibolite bodies to the west of the complex (Figure 2) as klippen, implying a direct relationship to the rocks of the complex. The fault is well exposed in the Chunky Gal Mountain roadcut along U.S. Route 64. There is an abrupt change in foliation at the fault contact, and both the amphibolite and biotite gneiss are cataclastically deformed to some degree. Along the fault contact the amphibolite forms a mylonite, according to the classification scheme of Higgins (1971). Only very near the fault contact has the amphibolite suffered recrystallization, retrogradation and mylonitization, while the gneiss appears mylonitic for several meters distance from the fault. This difference in behavior between the two lithologies may be due to factors discussed by Waters and Campbell (1935). Under the pressure-temperature conditions that result in the formation of a mylonite from graywackes, mafic rocks such as diabases and basalts are partially recrystallized (Waters and Campbell, 1935). This reasoning can logically be applied to the metamorphic equivalents of the above described rocks. Similar mylonites formed from mafic gneisses have been described by Sclar (1958).

Several petrographic traverses were made from gneiss into amphibolite along the southern portion of the complex. The gneisses

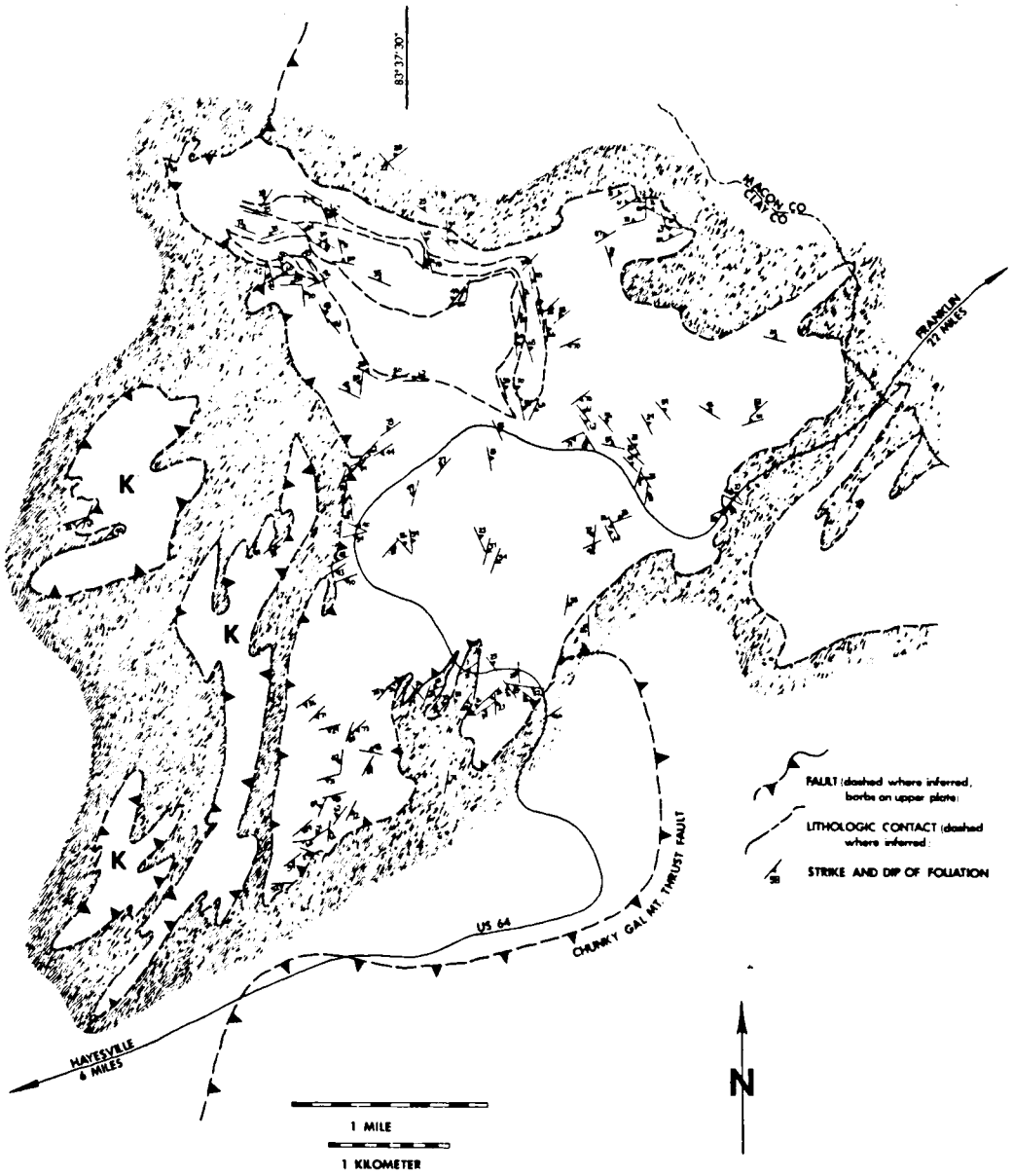

Figure 2. Structure map of the Chunky Gal Mountain complex showing strike and dip measurements of axial planar (S_2) foliation. Patterned area represents Carolina Gneiss and indicates the limits of the study area only, and does not represent orientation of rock fabric. The Carolina Gneiss-amphibolite contacts and the placement of the Chunky Gal Mountain thrust fault are modified after Hatcher (in Hatcher and Butler, 1979). Amphibolite bodies marked by K are klippen.

become more intensely deformed as the contact is approached, and they contain progressively more crushed hornblende porphyroclasts, which bear features similar to those described in hornblende porphyroclasts from the Grenville Front (Allison and LaTour, 1977). On the basis of float, similar to that just described, the Chunky Gal Mountain thrust fault is thought to extend northward along the amphibolite-gneiss contact, as postulated by Hatcher and Butler (1979) and shown in Figure 2. The contact along the northern portion of the complex is sharp, but does not appear in outcrop to be a fault (Kuntz, 1964). Although highly weathered, the eastern contact between the amphibolite and gneiss along U.S. Route 64 appears to be a fault, as shown by an abrupt change in orientation of foliation and the presence of a mylonitic fabric in the gneiss. Amphibolites on Riley Knob (Plate I) contain boudinaged hornblende grains, in thin section, similar to those observed along the southern contact. It appears as though the complex may be almost, or entirely fault-bounded, with the Chunky Gal Mountain thrust fault along the southern and possibly western to northwestern contacts, and one or more unnamed faults along the eastern to northeastern contacts.

Mafic-Ultramafic Contacts

The contact of the ultramafic rocks with the amphibolite is everywhere concordant with the foliation developed in the amphibolite, and no thermal aureole has been observed. The dunite is sheathed by a narrow zone of talc-chlorite schist that is variable in width, and which exhibits a very strong foliation, slickensided surfaces, and minor

folds and crenulations produced by shearing movements (Kuntz, 1964). The foliation and slickensided surfaces are parallel to the contact. Minor folds in the amphibolite appear to have an east-southeast vergence along the western margins of the ultramafic body, and a north-northwest vergence along the eastern margins. All minor folds plunge northeast. Kuntz (1964) reported parting surfaces in the dunite, caused by many closely spaced fractures which pass through olivine grains. The partings in the dunite and the foliation of the talc-chlorite schists have orientations parallel to the contact and to the foliation observed within the enclosing amphibolite.

Kuntz (1964) stated that the envelope rocks are never sheared or fractured near the contact; however, this is not always the case. Several petrographic traverses have revealed a zone of cataclasis, albeit discontinuous, within the amphibolite near the contact. The relict foliation to which Kuntz (1964) referred is more likely a penetrative fabric derived from shear along the contact while the rocks were under a high confining pressure. Ramberg (1956), in studies emphasizing the relation between chemical composition and the manner of deformation under high-grade metamorphic conditions, found that ultramafic rocks are much more likely to rupture than amphibolites under the same conditions. This may at least partially explain the different behaviors of the two rock types near the contact. Griggs et al. (1958) showed that hard rocks under high confining pressure (5 kb), and subjected to differential stress, deform largely through cataclastic flow with minor internal gliding. The deformation is largely concentrated at

localized shear zones. This may explain why the cataclastic zone in the amphibolite is of a restricted nature. Localized shear may develop along the contact between two lithologies which behave differently in a stress field. Such a field could develop if the complex as a whole were being folded or tectonically emplaced. Alternatively, it could result from tectonic emplacement of dunite into the amphibolite protolith. This latter interpretation is consistent with the petrofabric studies of Sailor and Kuntz (1973) which showed that the mineral fabric within the dunite is not concordant with the foliation in the amphibolite. The ultramafic rocks were not cataclastically deformed, because they were protected by the talc-chlorite schist sheath, which deformed easily and dissipated most of the localized stress.

Structural Analysis

The dominant penetrative fabric at Chunky Gal Mountain is a foliation which is axial planar to early isoclinal folds. Strike and dip measurements of this foliation are shown in Figure 2. It can be readily seen from the orientation of this axial planar foliation that the isoclinal folds have been deformed. These early folds, which are passive flow isoclinal to isoclinal recumbent, trend east-west to east-northeast. They have been refolded by northeast striking flexural-flow folds. The early isoclinal system and the later flexural flow system appear to correspond to Hatcher and Butler's (1979) regional F_2 and F_3 events, respectively. F_1, which is also an isoclinal recumbent fold system striking east-west to east-northeast and verging north to

northeast, is rarely observed in this area and is commonly transposed (Hatcher and Butler, 1979). In any case S_2 is the dominant foliation in this area, and the axial planar penetrative fabric observed at Chunky Gal Mountain is hereafter referred to as S_2.

Poles to the 265 measurements of the axial planar (S_2) foliation, contoured on a Schmidt diagram (Figure 3), show a distinct girdle which is due to refolding of the earlier isoclines by the later flexural-flow folds. When poles to axial surfaces of the later (F_3) folds are plotted, they form a cluster on the girdle, while fold axes of these later folds cluster around a point, β (N60E26NE), which is also the pole to the plane formed by the girdle (Figure 3). This clearly indicates that there are two dominant fold systems affecting the complex: one, an early isoclinal system (F_2) which developed a penetrative axial planar foliation (S_2); and the other, a later flexural-flow system (F_3) which developed no such penetrative fabric. Later crenulations, Hatcher and Butler's (1979) F_4 folds, are observed locally within the complex.

Interference patterns developed at culminations of interfering fold systems are observed on all scales, from hand sample to map scale. In plan view (Figure 2) the complex as a whole bears a striking resemblance to a Ramsey Type II interference pattern (Ramsey, 1967).

Faulted contact relationships between the amphibolite and Carolina Gneiss indicate a tectonic mode of emplacement for the amphibolite. The contact between the mafic and ultramafic units is a sheared serpentinite, and localized but discontinuous cataclasis is developed in amphibolite near the serpentinite. The discontinuous zone of cataclasis observed in

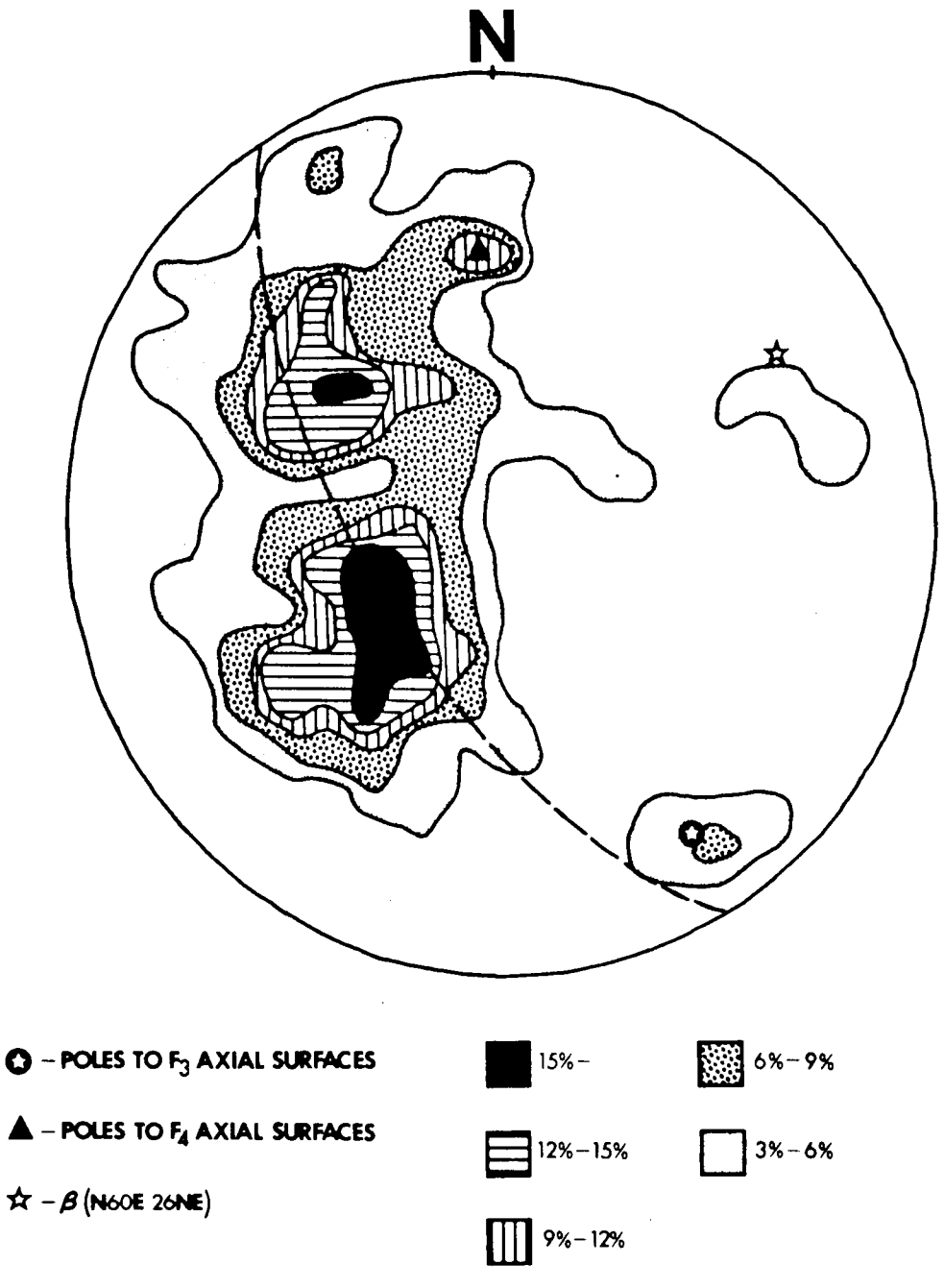

Figure 3. Schmidt contour diagram of poles to 265 measurements of axial planar (S_2) foliation in Chunky Gal Mountain amphibolites. The dashed line represents the fold girdle formed by poles to S_2 foliation measurements. β is the pole to the plane formed by the fold girdle. The solid circle with the star inside represents an average of nine measurements of F_3 (flexural-flow) axial surfaces, while the closed triangle represents an average of five measurements of F_4 (crenulation) axial surfaces.

the amphibolite may have been produced either by differential stress along the contact during tectonic emplacement of both lithologies simultaneously as intercalated sheets, or by diapiric emplacement of the ultramafic body into the amphibolite. Foliations in the amphibolite are concordant with partings in the dunite, indicating that both units suffered similar deformation subsequent to emplacement of the ultramafic.

CHAPTER III

PETROGRAPHY AND MINERALOGY

Mafic Envelope Rocks

Based on mineral assemblages, textural relationships, and geothermometry, the amphibolites have been broadly divided into two types, designated I and II. Their distribution (Figure 1, p. 2) appears to be structurally controlled. Type I amphibolites are generally restricted to the eastern portion of the complex, which may be the down-plunge direction of a large scale antiformal flexural-flow (F_3) fold; Type II amphibolites are generally found in the western portion of the complex. The line separating these two rock types may then approximate the surface trace of a large-scale, early isoclinal (F_2) axial plane. Because of the apparent differences in metamorphic grade between Types I and II amphibolites, it is also possible that they are in faulted contact; however, no field evidence for such a fault was observed.

Petrography

Typical equilibrium assemblages for both amphibolite types are shown on ACF projections in Figure 4.

Type I amphibolites are typically medium- to coarse-grained and granoblastic (Figure 5a) with a "salt and pepper" appearance in hand specimen. The penetrative S_2 fabric is only weakly expressed in these amphibolites. Hornblende and plagioclase form a homogeneous diablastic intergrowth; however, hornblende prisms, although exhibiting random

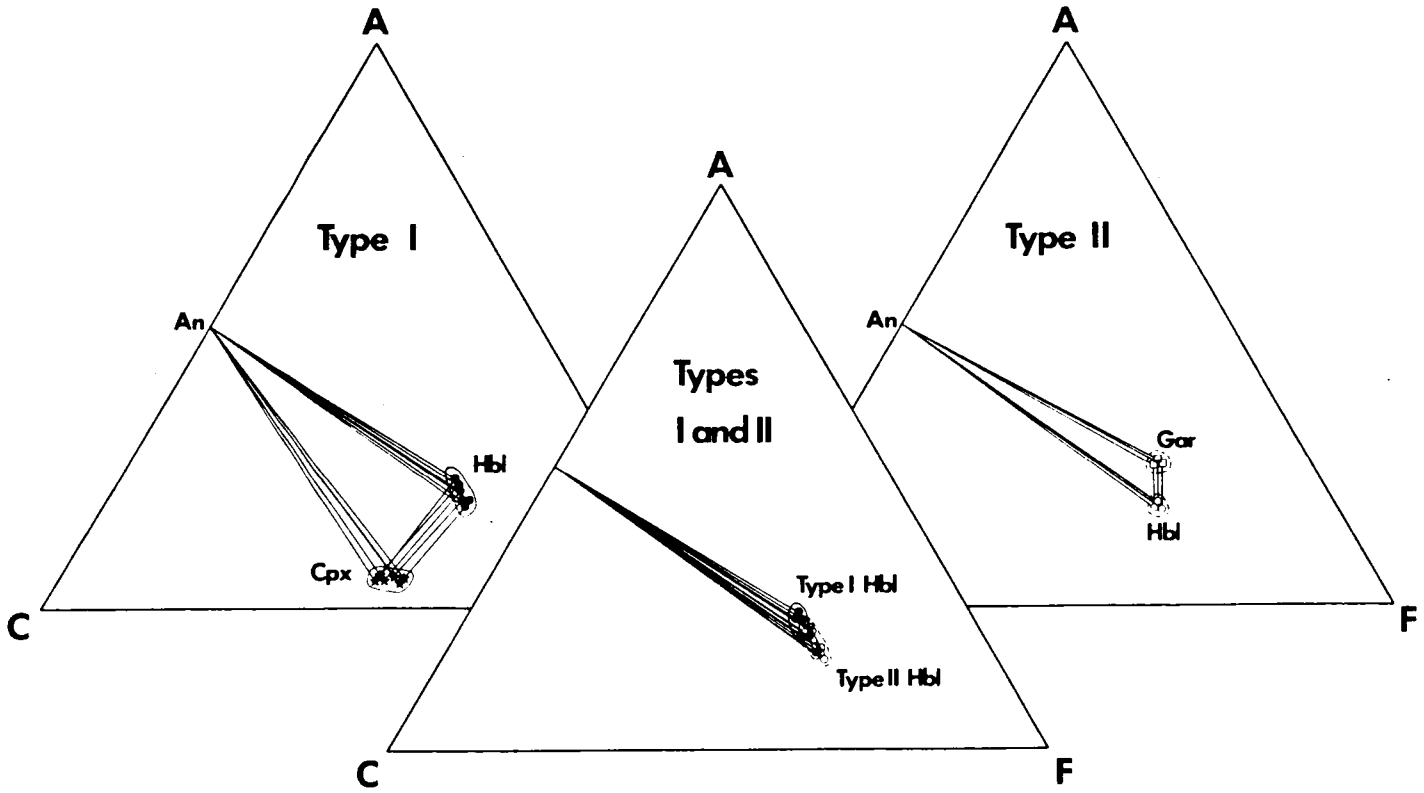

Figure 4. ACF diagrams showing assemblages found only in Type I and Type II amphibolites, and assemblages common to both types. Solid symbols and lines represent Type I amphibolites, and open symbols with dashed lines represent Type II amphibolites throughout the paper. Mineral abbreviations correspond to: the anorthite component in plagioclase (An), clinopyroxene (Cpx), hornblende (Hbl), and garnet (Gar).

Figure 5. Photomicrographs of mafic and ultramafic lithologies, in plane polarized light except where noted otherwise. Scales are shown at bottom of figure. (a) Granoblastic texture commonly observed in Type I amphibolites. Note distinct grain boundaries which are straight to slightly curved. (b) Common appearance of the Type I oxide assemblage showing a grain of magnetite (M) adjacent to a hemo-ilmenite (I)/ilmeno-hematite (H) grain. Both of the latter phases contain oriented lamellae of the complimentary phase, and a later set of hematite lamellae which transect both phases. Reflected light with crossed nicols. (c) Poly-deformational fabric often observed in Type II amphibolites. The S_2 foliation (parallel to the long dimension of the amphiboles) is folded by a crenulation oriented diagonally in the photograph. (d) Euhedral titanite common in Type II amphibolites. (e) Dunite exhibiting recrystallized fabric. Crossed nicols. (f) Olivine-rich troctolite showing corona structure.

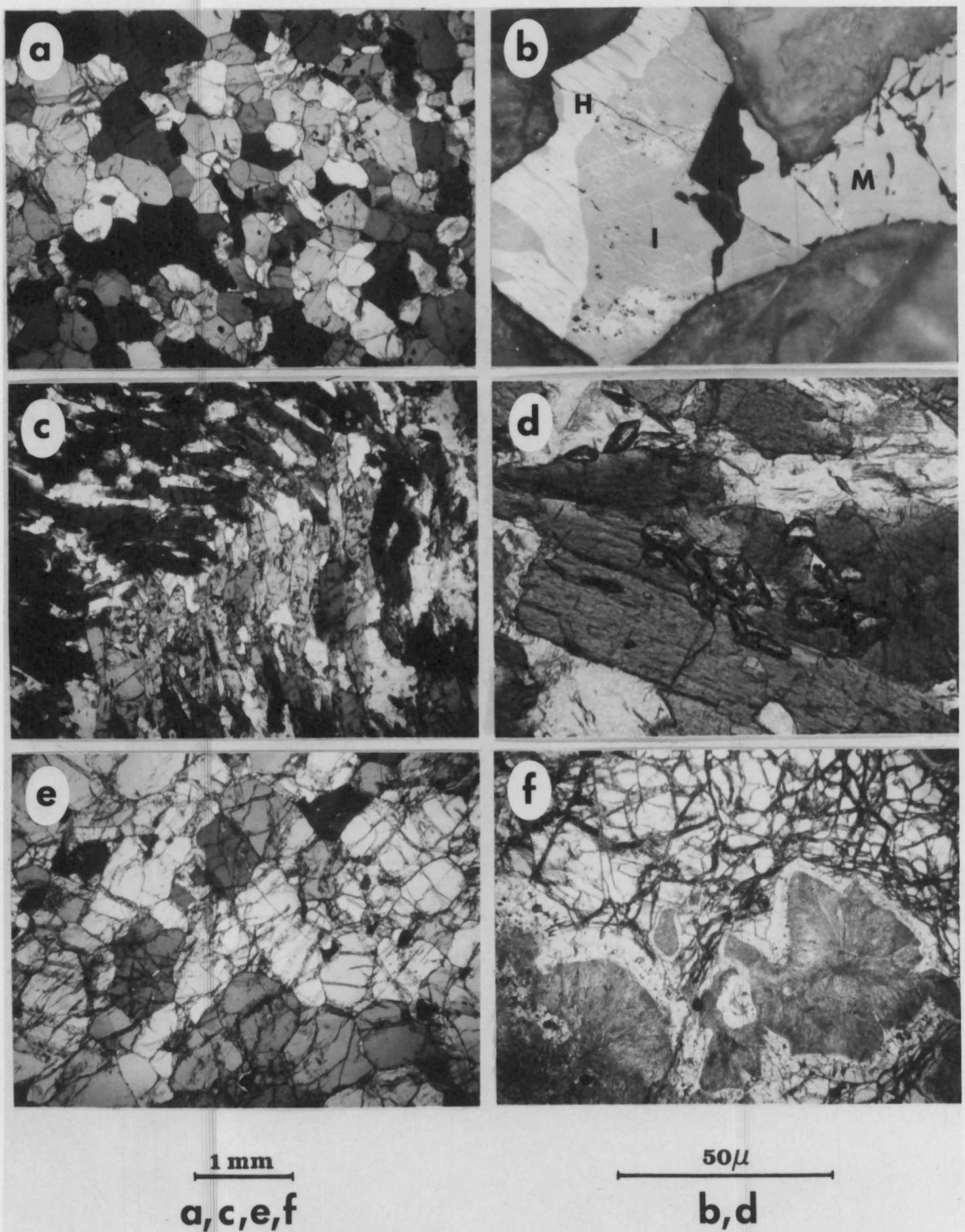

Figure 5.

spatial distribution, define a mineral lineation which lies within the plane of the S_2 foliation. Rarely is evidence for more than one deformational episode observed in any Type I amphibolite. Many samples do show evidence of cataclasis such as recrystallized mylonitic fabrics or, in hand specimen, the presence of coherent crush breccias (Higgins, 1971). Mineral grains in many Type I amphibolites show undulose extinction. Strain has commonly been relieved by deformation twinning in plagioclase and hornblende, the development of en echelon lattice dislocations in plagioclase, and subgrain recrystallization in quartz.

The major assemblages found in Type I rocks are hornblende-plagioclase, and hornblende-plagioclase-clinopyroxene. Accessory minerals include quartz, scapolite, calcite, magnetite, ilmenite, hematite, rutile, pyrite and pyrrhotite. Grain boundaries are typically straight to slightly curved and are often parallel to {110} of hornblende. These boundaries are well-developed and tend to be unilateral rational with equilibrium interfacial angles. Hornblende is pleochroic from brown or reddish brown (Z) to greenish brown (X) and is free of inclusions. Small euhedral grains of interkinematic (in relation to F_2 and F_3) hornblende occur in several Type I samples and are of the same composition as the more common synkinematic hornblende. Plagioclase grains are generally equant to slightly rounded, unzoned or slightly zoned, and often show well developed polysynthetic and strain-induced twins. Many specimens exhibit prograde breakdown of plagioclase to scapolite. Quartz occurs as an accessory phase and is commonly xenoblastic with abundant included needles of rutile. Rutile also

occurs as discrete grains in some samples and is commonly twinned on {011}. The presence of rutile in Type I rocks versus titanite (sphene) in Type II rocks, although not an unabmiguous correlation, does seem to suggest that Type I amphibolites are of a higher grade than Type II amphibolites (Wenk and Keller, 1969). Pyrite and pyrrhotite are very minor and commonly occur along cleavage faces in hornblende, and as rounded blebs along grain boundaries. The common opaque oxide minerals are hemo-ilmenite, ilmeno-hematite, and magnetite, which is a common upper-amphibolite grade assemblage (Rumble, 1973; Dougan, 1974). Magnetite occurs as discrete grains showing minor oxidation lamellae of hematite along rims, and as grains in mutual contact with hemo-ilmenite/ilmeno-hematite grains. The contact is always between hemo-ilmenite and magnetite, never ilmeno-hematite and magnetite. Ilmeno-hematite hosts contain many blebs of hemo-ilmenite and ferrian-ilmenite, some of which have altered to leucoxene. In several grains, half of the grain is composed of hemo-ilmenite host with ilmeno-hematite blebs and the other half is ilmeno-hematite host with hemo-ilmenite blebs (Figure 5b), suggesting simple sub-solvus exsolution. These grains often contain octahedral lamellae of almost pure hematite passing through both host phases. The opaque phases are generally minor constituents; however, in some samples they constitute up to 5% of the rock.

Type II amphibolites are characterized by well-developed axial planar (S_2) foliation, the common appearance of two or more deformational fabrics (Figure 5c), and a propensity for marked textural variation,

even within thin-section areas. They vary from fine- to coarse-grained and are typically inequigranular, with elongate prisms of hornblende and small ragged xenoblastic plagioclase and quartz grains. It is quite common to observe abrupt changes from fine-grained to coarse-grained amphibolite within a 1-2 mm range. This feature may reflect original layering, suggesting that these amphibolites possibly represent cumulate gabbros (Mevel et al., 1978). Alternatively, presence of striped or banded amphibolites may be due to metamorphic differentiation (Evans and Leake, 1960). The occurrence of striped amphibolites is erratic, and the stripes can only be traced for several meters along strike.

Common assemblages in Type II amphibolites include epidote-plagioclase-hornblende, plagioclase-hornblende, and plagioclase-garnet-hornblende. Accessory minerals include quartz, titanite, clinozoisite, pyrite, pyrrhotite, and apatite. Amphiboles are pleochroic, either from brown (Z) to yellow green (X) or from dark green (Z) to bluish green (X). Grain boundaries are commonly ragged and indistinct, and most phases contain abundant inclusions. Hornblende is often poikiloblastic with inclusions of quartz, epidote, and plagioclase. Plagioclase has developed into spherical, low surface energy shapes (Spry, 1969) during posttectonic crystallization. Many epidote grains and some hornblende grains show evidence of posttectonic crystallization; however, this growth occurred before development of the F_4 crenulation. Garnet porhyroblasts are commonly rolled and contain inclusions of hornblende and epidote. S_i of the garnet inclusion trains is conformable

to S_2 foliation of the rock. Near the western contact of the amphibolite with the Carolina Gneiss, many epidote grains contain metamict allanite cores. Epidote-group minerals including epidote, clinozoisite, and allanite appear to be mainly primary and syntectonic (in relation to F_2), but they also occur as retrograde minerals, as discussed below. Euhedral titanite (Figure 5d) is an abundant accessory mineral and is often concentrated along F_4 hinge zones. In several samples leucoxene appears to be pseudomorphous after titanite.

A retrograde event of middle to upper greenschist grade has affected rocks of the entire complex and the effects are noticeable and widespread, albeit of patchy distribution. Retrograde products include chlorite after hornblende, uralite after pyroxene, idioblastic epidote and clinozoisite, sericite, and poikiloblastic actinolite, all with random orientations. An interesting reaction observed in both amphibolite types occurs at plagioclase-hornblende grain boundaries and produces an epidote-quartz symplectite. Similar reactions have been described by Tobisch (1968) and Mehta (1976). The epidote (± clinozoisite) is concentrated mostly in the plagioclase, where it may form a graphic intergrowth with plagioclase and a vermicular intergrowth with released quartz. Occasionally the quartz may form a vermicular intergrowth with the adjacent hornblende. Many late-stage brittle fractures occur within the amphibolite, particularly Type I, and are frequently mineralized. These fractures contain quartz, calcite, albite, and later void-filling chlorite. The amphibolite forms crackle breccia along the fractures, and breccia fragments can be seen altering to greenschists. Types I

and II amphibolites show similar retrograde effects with two exceptions: (1) Several Type I rocks show up to 20% retrograde epidote which occurs as an intergranular rimming phase throughout the rock. This rimming phase surrounds all pregreenschist phases and is composed of several large grains; (2) A unique reaction in Type I rocks is indicated by the presence of a reaction rim of epidote around scapolite, which contains remnants of plagioclase within its core. This would suggest that scapolite, in this case, is a higher temperature alteration product of plagioclase (Shaw, 1960; Orville, 1975; Goldsmith and Newton, 1977).

Mineral Chemistry

Representative analyses of minerals are presented in Tables 1 and 2. Further mineral analyses are reported in Appendix B. The compositions of coexisting major phases are shown in a Ca-Mg-Fe ternary diagram and accompanying Ab-An diagram in Figure 6.

Amphiboles are all calcic, with $(Ca + Na)_B \geqslant 1.34$, and are plotted on the nomenclature diagrams for calcic amphiboles from Leake (1978) (Figure 7). Observed chemical variations among amphiboles are gradational, although a distinct separation of Type I and Type II amphiboles can be made, with $Mg/(Mg + Fe^{2+})$ higher in Type I amphiboles. A similar increase was observed in hornblendes from the Adirondacks (Engel and Engel, 1962), as metamorphic grade increased from almandine-amphibolite to hornblende-granulite facies. They also observed an increase in Ti with increasing grade. The Ti content of hornblendes in Chunky Gal Mountain amphibolites, when plotted as a histogram (Figure 8), shows two modes which in general correspond to Type I (higher-Ti) and

Table 1. Representative Microprobe Analyses of Coexisting Minerals in Amphibolites

	Type I Amphibolites					Type II Amphibolites							
	sample 6am34			sample 12-1		sample 4-10			sample 2-18			Sample 8-9	
	Hbl	Plag	Cpx	Hbl	Plag	Hbl	Plag	Epid.	Hbl	Plag	Gar	Hbl	Plag
SiO_2	43.68(7)[b]	54.9(5)	49.9(1)	45.1(1)	49.2(4)	44.1(1)	62.6(3)	37.7(1)	45.1(3)	60.1(3)	38.0(3)	43.4(1)	62.1(2)
TiO_2	0.92(5)	--	0.29(2)	1.11(7)	--	0.42(4)	--	0.12(2)	0.58(2)	--	--	0.59(3)	--
Al_2O_3	12.8(3)	28.9(1)	4.9(1)	12.2(1)	32.3(1)	11.9(3)	24.5(1)	26.5(5)	12.1(2)	25.2(2)	21.3(2)	12.51(1)	24.4(2)
Cr_2O_3	n.d.	--	n.d.	n.d.	--	n.d.	--	--	n.d.	--	n.d.	n.d.	--
FeO	9.3(2)	--	9.3(1)[d]	11.2(2)	--	11.2(1)	--	7.2(2)[d]	15.4(1)	--	21.2(2)	10.1(2)	--
Fe_2O_3[a]	6.6(2)	--	--	4.1(2)	--	3.1(1)	--	--	1.2(1)	--	--	6.06(2)	--
MnO	0.20(1)	--	0.25(3)	0.29(4)	--	0.22(5)	--	0.11(2)	0.08(1)	--	2.1(3)	0.21(5)	--
MgO	11.4(1)	--	12.2(1)	11.5(2)	--	11.4(1)	--	0.09(1)	9.8(1)	--	1.9(1)	10.7(2)	--
CaO	11.4(1)	10.88(6)	23.1(2)	11.9(1)	15.1(2)	11.64(7)	5.30(7)	23.4(1)	12.03(9)	6.4(2)	14.1(3)	11.3(1)	5.5(1)
Na_2O	1.89(9)	5.42(7)	0.70(4)	1.75(9)	2.9(2)	1.9(1)	8.32(9)	n.d.	1.36(2)	7.8(3)	--	1.63(4)	8.4(1)
K_2O	0.32(2)	n.d.[c]	n.d.	0.26(2)	n.d.	0.58(7)	0.08(1)	n.d.	0.62(5)	0.07(1)	--	0.63(3)	0.07(0)
Total	98.61	100.16	100.86	99.72	99.66	96.63	100.88	95.39	98.40	99.71	99.63	97.27	100.55
Formula Basis (oxygens)	23	8	6	23	8	23	8	25	23	8	12	23	8
Si	6.352	2.468	1.862	6.498	2.254	6.553	2.745	6.120	6.642	2.681	2.999	6.427	2.736
Ti	0.101	--	0.007	0.120	--	0.047	--	0.014	0.064	--	--	0.066	--
Al^{IV}	1.650	1.531	0.217	1.500	1.745	1.450	1.269	5.070	1.360	1.325	1.982	1.570	1.268
Al^{VI}	0.540	--	--	0.580	--	0.630	--	--	0.740	--	--	0.610	--
Cr	n.d.	--	n.d.	n.d.	--	n.d.	--	--	n.d.	--	n.d.	n.d.	--
Fe^{2+}	1.134	--	0.290	1.348	--	1.390	--	0.979	1.897	--	1.398	1.252	--
Fe^{3+}	0.725	--	--	0.449	--	0.348	--	--	0.143	--	--	0.674	--
Mn	0.025	--	0.007	0.035	--	0.028	--	0.014	0.099	--	0.141	0.026	--
Mg	2.478	--	0.678	2.467	--	2.543	--	0.018	2.156	--	0.231	2.360	--
Ca	1.778	0.523	0.925	1.846	0.740	1.852	0.248	4.075	1.898	0.309	1.250	1.795	0.260
Na	0.533	0.472	0.050	0.488	0.257	0.559	0.706	n.d.	0.388	0.675	--	0.467	0.718
K	0.059	n.d.	n.d.	0.048	n.d.	0.110	0.003	n.d.	0.116	0.004	--	0.119	0.002

[a] Fe_2O_3 calculated.

[b] Units in () represent one standard deviation of replicate analyses in terms of least units cited.

[c] n.d. = not detected; less than 0.03%.

[d] All Fe calculated as Fe^{2+}.

Table 2. Representative Microprobe Analyses of Accessory Minerals in Amphibolites

	sample 8-15		6am34		6am34			6am34		8-9
	Scap	Scap	Mag	Mag	Mag -	Ilm -	Hem	Ilm -	Hem	Sphene
SiO_2	46.9(2)[b]	47.2(4)	--	--	--	--	--	--	--	30.49(3)
TiO_2	--	--	0.19(2)	0.09(2)	0.43(5)	46.5(5)	18.7(8)	47.0(6)	14.6(5)	39.2(1)
Al_2O_3	26.08(7)	26.38(6)	0.42(7)	0.51(7)	0.36(0)	0.07(2)	0.14(3)	0.07(2)	0.35(1)	0.91(3)
Cr_2O_3	--	--	0.25(4)	0.29(4)	0.25(4)	0.03(0)	0.2(1)	n.d.	0.15(3)	n.d.
FeO	--	--	31.3(4)	31.3(7)	31.8(3)	40.6(4)	16.6(5)	39.5(3)	12.7(4)	0.54(7)[d]
Fe_2O_3[a]	--	--	67.6(4)	68.1(7)	67.98(3)	11.4(4)	63.6(5)	11.8(4)	71.0(7)	--
MnO	--	--	0.05(3)	0.08(5)	0.04(0)	0.8(1)	0.11(7)	1.4(9)	0.28(5)	n.d.
MgO	--	--	0.05(2)	0.14(1)	0.06(0)	0.3(1)	0.22(3)	0.85(4)	0.19(2)	n.d.
CaO	16.7(1)	16.45(8)	--	--	--	--	--	--	--	28.3(1)
Na_2O	4.08(6)	4.09(5)	--	--	--	--	--	--	--	--
K_2O	n.d.[c]	n.d.	--	--	--	--	--	--	--	--
Total	93.86	94.15	99.90	100.54	100.98	100.01	99.70	100.71	99.38	99.53
Formula Basis (oxygens)	8	8	4	4	4	3	3	3	3	10
Si	2.320	2.321	--	--	--	--	--	--	--	1.999
Ti	--	--	0.005	0.003	0.012	0.887	0.368	0.885	0.290	1.933
Al^{IV}	1.518	1.528	0.019	0.023	0.016	0.002	0.004	0.002	0.011	0.069
Al^{VI}	--	--	--	--	--	--	--	--	--	--
Cr	--	--	0.008	0.009	0.008	0.001	0.004	n.d.	0.003	n.d.
Fe^{2+}	--	--	1.007	0.999	1.013	0.860	0.363	0.827	0.279	0.029
Fe^{3+}	--	--	1.956	1.957	1.946	0.218	1.250	0.223	1.404	--
Mn	--	--	0.002	0.003	0.001	0.018	0.024	0.030	0.006	n.d.
Mg	--	--	0.003	0.008	0.003	0.015	0.009	0.032	0.007	n.d.
Ca	0.884	0.865	--	--	--	--	--	--	--	1.993
Na	0.390	0.389	--	--	--	--	--	--	--	--
K	n.d.	n.d.	--	--	--	--	--	--	--	--

[a] Fe_2O_3 calculated.

[b] Units in () represent one standard deviation of replicate analyses in terms of least units cited.

[c] n.d. = not detected; less than 0.03%.

[d] All Fe calculated as Fe^{2+}.

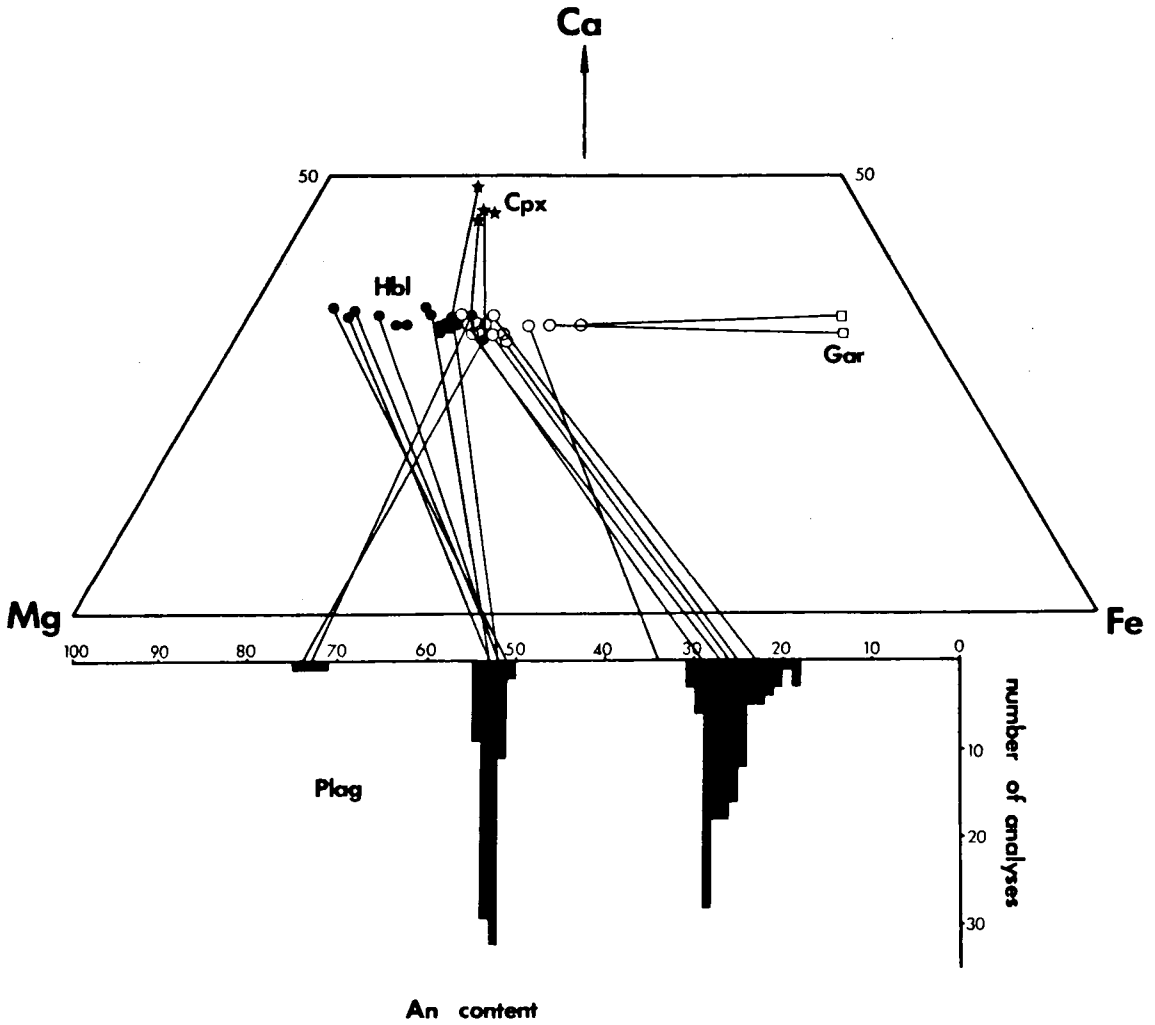

Figure 6. Ca-Mg-Fe and plagioclase feldspar (Ab-An) diagrams, in mole percent, showing representative mineral analyses from several Type I (filled symbols) and Type II (open symbols) amphibolites. Coexisting phases are shown with tie lines. The Ab-An histogram shows all plagioclase analyses (an average for each grain) from the Chunky Gal Mountain amphibolites.

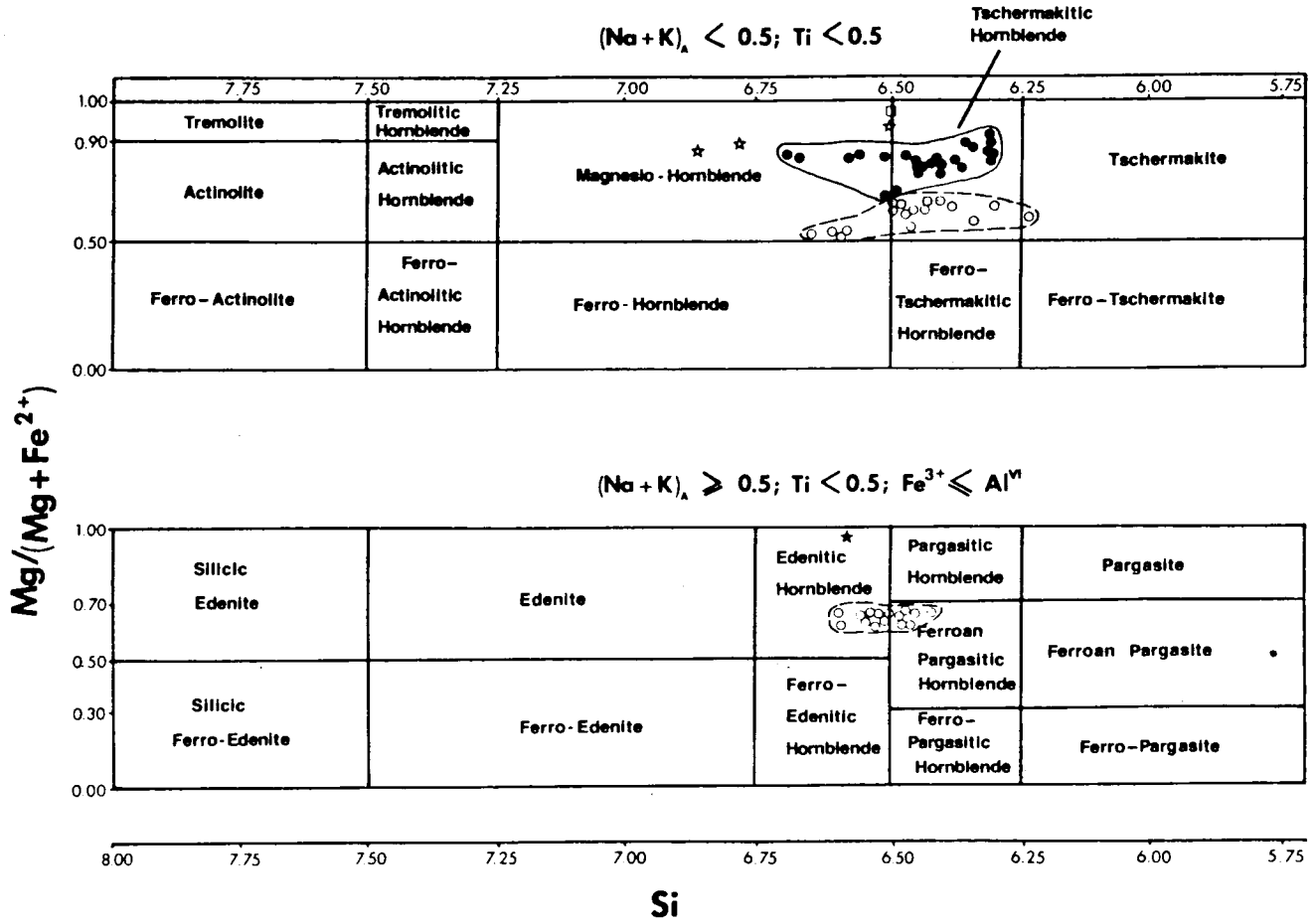

Figure 7. Nomenclature diagram for calcic amphiboles from Leake (1978). Filled circles are Type I amphiboles, open circles are Type II amphiboles, closed stars are amphiboles from the dunite, open squares are amphiboles from the corona in the troctolite, and open stars represent amphiboles from the troctolite-amphibolite.

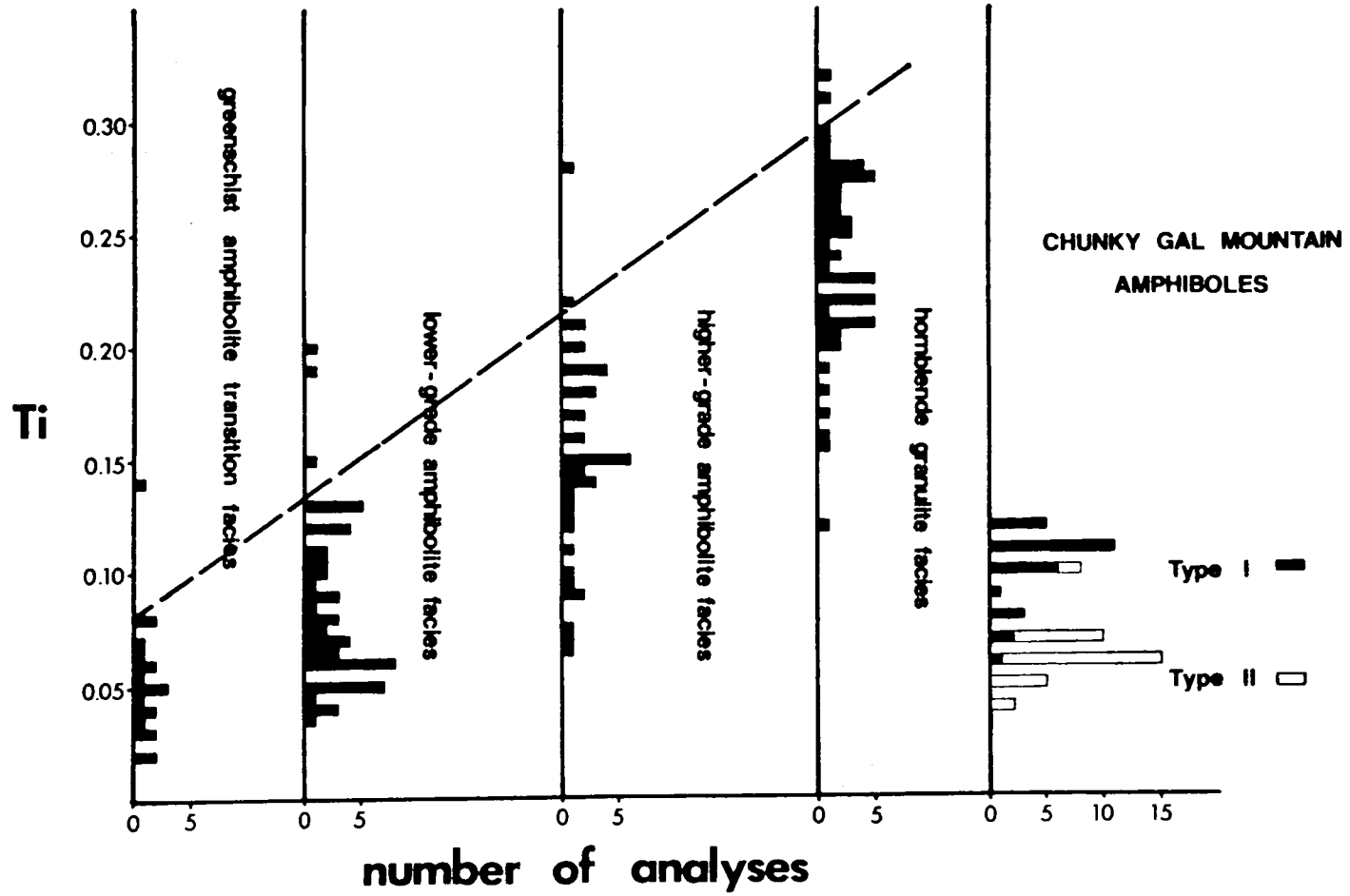

Figure 8. Histogram of Ti contents (in weight percent) from Raase (1974) and a histogram of Ti contents in amphiboles from Chunky Gal Mountain (far right of diagram).

Type II (lower-Ti) amphibolites. Raase (1974) has shown that the Ti content of amphiboles generally increases with increasing grade (Figure 8), but the absolute Ti contents are highly dependent upon variation in bulk rock Ti content as well as coexisting Ti-bearing phases. The Ti contents of both Type I and Type II amphibolites are low, resulting in a lower apparent grade of metamorphism. Another important constraint on Ti content in amphiboles is the oxygen fugacity under which they crystallized (Spear, 1977). Type I amphiboles crystallized at higher temperatures than Type II amphiboles (see Geothermometry and Geobarometry) and they show an expected increase in Ti content; however, they also experienced higher oxygen fugacities (see Petrogenesis, Metamorphism) which tended to lower the Ti content. The combined factors of temperature, oxygen fugactiy and bulk rock Ti content limit the usefulness of Raase's (1974) Ti diagram to generalizations about metamorphic grade. Na^{M4}, Al^{IV}, and $(Al^{VI} + Fe^{3+} + Ti + Cr)$ all show an increase from Type II to Type I amphiboles (Figure 9), although the two fields do overlap. Laird and Albee (1981) showed similar increases in the same elements with increasing metamorphic grade for amphiboles from Vermont, and attributed this to an apparent increase in substitution of both the tschermakite and glaucophane components within the amphibole structure. This is supported by the compositions of amphiboles from Chunky Gal Mountain. Laird and Albee (1981) also found that Na and K in the A site decrease with increasing grade, suggesting a decrease in edenite substitution within the amphibole lattice. This decrease in A site alkalis with increasing grade is also observed at Chunky Gal Mountain (Figure 9) along with a concomitant rise

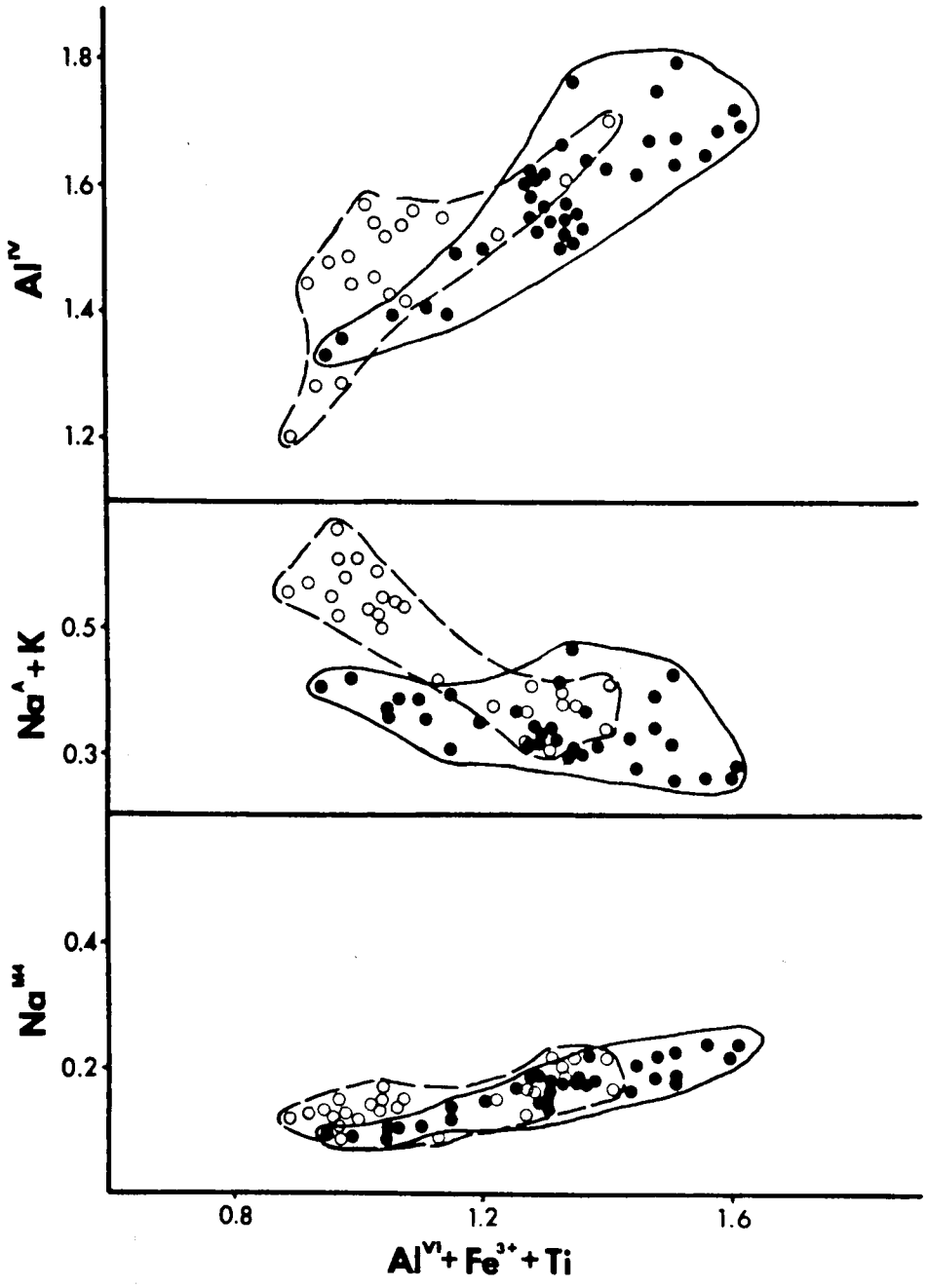

Figure 9. Plots of Na^{M4}, $(Na + K)_A$, and Al^{IV} versus $Al^{VI} + Fe^{3+} + Ti$ in cation percent. Filled symbols are Type I and open symbols are Type II amphiboles respectively. Na^{M4} and Al^{IV} increase with metamorphic grade, while $(Na + K)_A$ decreases.

in M4 site occupancy by Na (Figure 9). Type I amphiboles are typically all pleochroic brown and brownish red (Z) to green brown (X) and have very little H_2O as suggested by high totals (e.g., 98.4%-99.7%) for other components. These amphiboles are similar to the brownish, hydroxyl-deficient hornblendes found in Adirondack granulites (Engel and Engel, 1964). However, Engel and Engel (1962), in their study of Adirondack amphibolites, noticed an increase in Na and K in the A site of amphiboles with increasing grade. In general, Type II amphiboles have low totals (e.g., 96.1%-98.1%) in comparison with Type I amphiboles, which suggests that they are richer in volatile components (principally H_2O). Amphiboles are unzoned and coexisting equilibrium amphibole compositions have not been found in any samples. Energy dispersive analysis of hornblendes revealed that H_2O is essentially the only volatile constituent.

Plagioclase compositions in Type II amphibolites vary from An_{19} to An_{31} with a majority around An_{29} (Figure 6). The variations in plagioclase compositions are probably due to coexisting epidote-group minerals. Primary epidote and clinozoisite have a direct effect upon plagioclase, causing it to be more calcic (Wenk and Keller, 1969) than plagioclase in assemblages which do not contain primary epidote-group phases. One sample each of Type I and Type II amphibolites was examined in detail with the electron microprobe to check for coexisting plagioclase compositions. Neither sample contained coexisting plagioclases, as observed in some other amphibolites (e.g., Wenk and Keller, 1969; Spear, 1980). The average composition of Type II

plagioclase, calcic oligoclase to sodic andesine, lies above Wenk and Keller's (1969) An_{17} + hornblende isograd, well within the amphibolite facies, and probably corresponds to a kyanite- (Turner, 1981) or possibly sillimanite-bearing pelitic assemblage. Plagioclase compositions in Type I amphibolites are either sodic-labradorite or sodic-bytownite with no gradation between groups and only very narrow ranges of An content within each group (Figure 6, p. 28). Only one sample contained zoned plagioclase (An_{78} core and An_{71-72} rim). In samples containing bytownite, the plagioclase poikiloblastically encloses tiny hornblende grains, which may represent hornblende relics left from prograde alteration of amphibole to calcic plagioclase and pyroxene. These plagioclase compositions are common in the upper-amphibolite facies, where the zone of labradorite-pyroxene amphibolites agrees with the sillimanite-almandine-orthoclase subfacies of Wenk and Keller (1969), and in mafic granulites, such as those described by Engel and Engel (1962) in the Adirondacks.

Garnets are present only in Type II assemblages. They are typically almandine with an appreciable grossular component. Irregular zoning patterns measured in two garnets from one sample indicate core and rim compositions of $Al_{47}Py_{6}Sp_{7}Gr_{40}$ and intermediate compositions of $Al_{58}Py_{8}Sp_{7}Gr_{27}$. This zoning pattern is defined solely by sympathetic variations in CaO and FeO.

The clinopyroxene in Type I amphibolites is salite (Figure 6) with an appreciable jadeite component, averaging about 12 mole percent. This composition falls within the range of salite compositions from

amphibolites associated with alpine-type ultramafics from the Dinaride ophiolite zone (Pamić et al., 1973) and is suggestive of a mafic igneous origin (Deer et al., 1978) for the Chunky Gal Mountain amphibolites.

Scapolite in Type I amphibolites ranges from Me_{68-93}. Energy dispersive analysis shows only a very minor sulfur peak and a trace chlorine peak. This and the presence of calcite at scapolite-plagioclase reaction points suggests that the scapolite belongs principally to the carbonate meionite-marialite solid-solution series. Analyzed epidotes in both types of amphibolite (Table 2, p. 27) are essentially pure $Ca_2(Al_{2.5}Fe_{0.5})(OH)(SiO_4)_3$ with trace amounts of Mn, Ti, and Mg. Compositions of coexisting oxide phases in the Type I assemblage are displayed in the FeO-Fe_2O_3-TiO_2 ternary (Figure 10). Host compositions of coexisting ilmeno-hematites and hemo-ilmenites are $Ilm_{95}Hem_5$ and $Ilm_{46-56}Hem_{54-44}$ respectively. Trace amounts of Mg, Mn, Al, and Cr are present in all analyzed oxide phases.

Ultramafic Rocks

Petrography

The most abundant ultramafic lithology found within the Chunky Gal Mountain complex is unaltered dunite, composed primarily of fine- to medium-grained anhedral olivine (Figure 5e, p. 20). Large relict phenocrysts of olivine occur rarely in the dunite and are often highly fractured. Granulation textures are widely developed in the dunite and have been described by Kuntz (1964). Patchwork extinction, deformation bands subparallel to {100}, and translation lamellae are also common

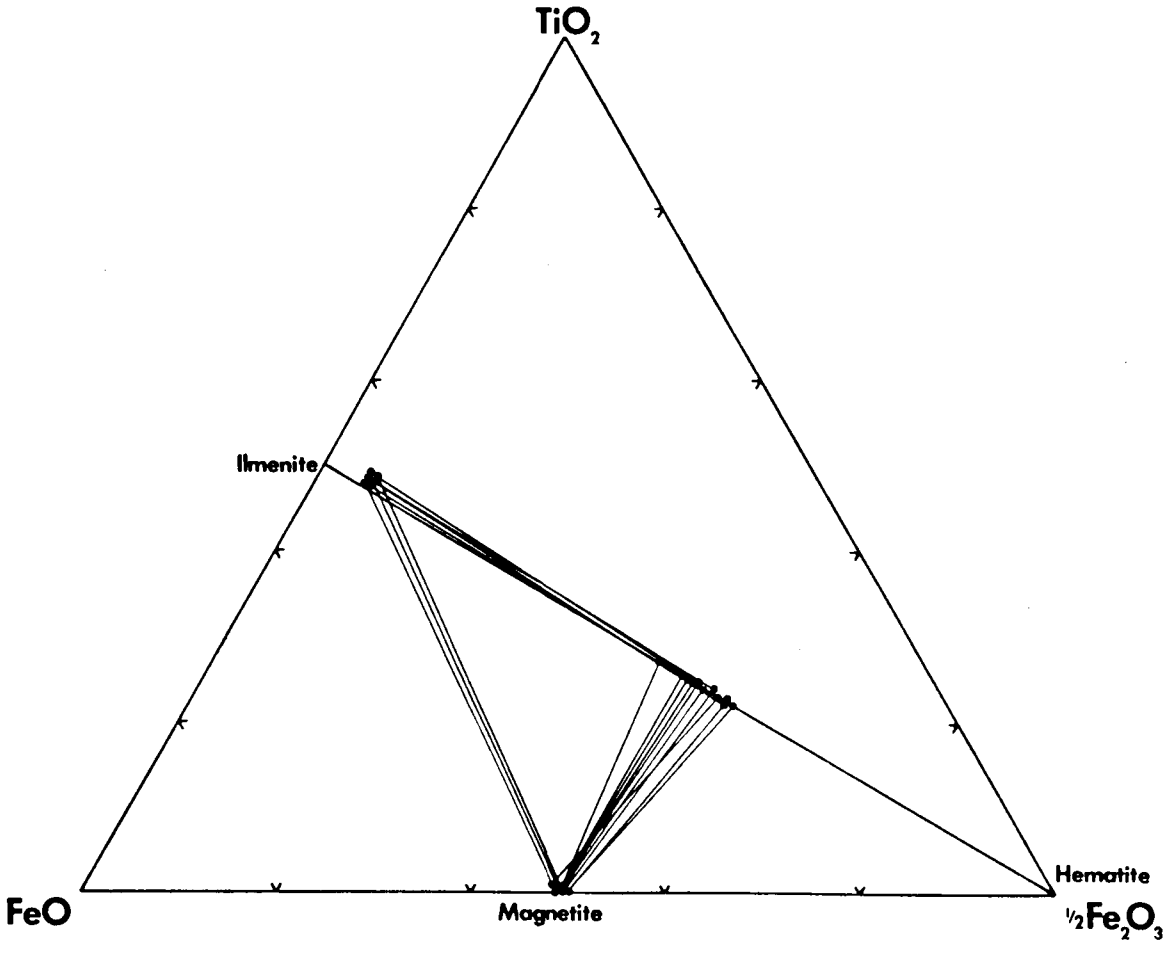

Figure 10. FeO-Fe_2O_3-TiO_2 ternary plot, in mole percent, of the Type I oxide assemblage. Coexisting compositions are shown with tie lines.

features (Kuntz, 1964). Sailor and Kuntz (1973) have shown that the orientation of the dunite fabric is unrelated to the amphibolite penetrative fabric (S_2 foliation). They suggested that the dominant fabric and the polygonal texture were developed by syntectonic recrystallization within the upper mantle.

Accessory minerals include: skeletal magnetite, often surrounded by chlorite; minor chromite, generally as inclusions in olivine; small, stubby uralitized diopsidic augites (not observed in this study but described by Kuntz, 1964); small crystals of edenitic hornblende showing apparent equilibrium boundaries with the olivine grains; and minor sulfides, including pyrite and pyrrhotite. The principal alteration products are felty mesh structures of talc and chrysotile, tremolitic amphibole, massive antigorite, and chlorite. In several of the smaller concordant ultramafic lenses, where serpentinization is almost complete, minor amounts of magnesite occur within the talc-chrysotile boxwork.

Troctolite is composed of varying amounts of olivine and plagioclase with accessory salitic pyroxene (Kuntz, 1964), chromite, and magnetite. Both chromite and magnetite occur as inclusions within olivine and plagioclase, and as discrete euhedral to subhedral grains. The most striking feature of troctolite is the well-developed corona texture, which occurs at all plagioclase-olivine boundaries (Figure 5f, p. 20). The coronas are composed of two distinct layers. The layer closest to olivine consists of stubby orthopyroxene prisms oriented normal to the boundary with olivine, and the layer closest to plagioclase consists of amphibole-spinel symplectite. Vermicular pleonaste intergrown with the

amphibole is oriented perpendicular to the contact. In places, the orthopyroxene is rimmed discontinuously by diopside; however, this is not a common feature. As modal olivine decreases, troctolite grades into anorthositic amphibolite composed of calcic plagioclase and minor corona minerals, mostly hornblende. All variations between these two end-members are observed.

Troctolite-amphibolite possesses a dominant gneissic structure and has been described by Hadley (1949) as containing relict corona texture. It is composed of plagioclase with varying amounts of olivine, amphibole, and clinopyroxene. Accessory minerals include corundum, chromite, magnetite and kyanite. The amphibole occurs as small crystals and as elongate prisms parallel to foliation. Kyanite is present where hornblende is a major constituent and often shows alteration to muscovite along its edges. Hadley's (1949) amphibole gneiss is composed of plagioclase and tschermakitic hornblende; it probably represents a more complete alteration stage of troctolite than the troctolite-amphibolite previously descirbed. Other alteration products of troctolite include talc-chlorite-serpentine rocks which are commonly schistose, but are sometimes massive and contain relict corona structures. The penetrative fabric observed in metatroctolites parallels S_2, and minor folds possess orientations similar to those observed in adjacent enveloping amphibolites.

Mineral Chemistry

Analyses are presented for mineral phases from three representative ultramafic lithologies in Table 3. Olivine grains from the dunite

Table 3. Representative Microprobe Analyses of Minerals in Ultramafic Rocks

	Dunite		Troctolite-Corona Traverse					Troctolite-Amphibolite	
	Oliv	Hbl	Plag	Hbl	Spinel	Opx	Oliv	Plag	Hbl
SiO_2	40.6(2)[b]	45.8(2)	45.3(1)	46.4(5)	0.91(2)	55.3(3)	40.5(1)	46.4(2)	47.7(6)
TiO_2	--	0.43(1)	--	n.d.	n.d.	n.d.	--	--	0.19(1)
Al_2O_3	--	11.2(1)	35.86(2)	15.1(4)	63.0(5)	0.79(6)	--	34.0(1)	10.8(3)
Cr_2O_3	n.d.[c]	n.d.	--	n.d.	n.d.	n.d.	n.d.	--	n.d.
FeO	11.5(5)[d]	1.7(1)	--	1.29(5)	5.27(3)	7.18(8)	9.9(1)	--	4.8(1)
Fe_2O_3[a]	--	2.9(1)	--	2.33(5)	6.09(3)	--	--	--	3.1(1)
MnO	0.12(2)	0.04(1)	--	n.d.	0.04(0)	0.17(2)	0.09(2)	--	0.13(2)
MgO	48.5(3)	18.7(1)	--	17.1(4)	19.6(5)	34.5(2)	49.8(4)	--	16.1(2)
CaO	n.d.	12.0(1)	18.9(1)	12.7(1)	1.43(2)	0.13(2)	n.d.	17.4(1)	12.58(7)
Na_2O	--	3.1(1)	0.6(1)	1.6(1)	1.23(1)	n.d.	--	1.6(1)	1.43(3)
K_2O	--	0.34(4)	n.d.	n.d.	0.04(2)	n.d.	--	n.d.	0.16(1)
TOTAL	100.85	96.49	100.75	96.77	97.73	98.19	100.44	99.57	97.35
Formula Basis (oxygens)	4	23	8	23	4	6	4	8	23
Si	0.993	6.543	2.070	6.500	0.023	1.955	0.990	2.145	6.786
Ti	--	0.046	--	n.d.	n.d.	n.d.	--	--	0.020
Al^{IV}	--	1.460	1.932	1.500	1.898	0.032	--	1.850	1.210
Al^{VI}	--	0.430	--	1.000	--	--	--	--	0.610
Cr	n.d.	n.d.	--	n.d.	n.d.	n.d.	n.d.	--	n.d.
Fe^{2+}	0.237	0.209	--	0.151	0.112	0.211	0.203	--	0.579
Fe^{3+}	--	0.313	--	0.246	0.117	--	--	--	0.340
Mn	0.002	0.005	--	n.d.	0.001	0.004	0.001	--	0.016
Mg	1.771	3.997	--	3.589	0.747	1.817	1.812	--	3.422
Ca	n.d.	1.835	0.928	1.916	0.039	0.004	n.d.	0.862	1.915
Na	--	0.866	0.056	0.440	0.061	n.d.	--	0.143	0.394
K	--	0.062	n.d.	n.d.	0.001	n.d.	--	n.d.	0.029

[a] Fe_2O_3 calculated.

[b] Units in () represent one standard deviation of replicate analyses in terms of least units cited.

[c] n.d. = not detected; less than 0.03%.

[d] All Fe calculated as Fe^{2+}.

sample have a very slight Fe-enrichment trend from core to rim. Compositions are Fo_{88-89} for olivines in the dunite near the periphery of the main ultramafic body; these values are close to those obtained optically by Kuntz (1964) for similarly placed dunite. He reports that the Fo content in olivine increases towards the core of the dunite body. Mineral analyses reported for the troctolite sample are from a traverse across a plagioclase-olivine contact, through a corona. The plagioclase is anorthite (An_{94}) and appears to be unzoned. The amphibole of the symplectite plots on the magnesio-hornblende/tschermakitic hornblende join (Figure 7, p. 29) of Leake's (1978) calcic amphibole diagram. This amphibole has been incorrectly described by previous workers (Hadley, 1949; Kuntz, 1964; Hartley and Penley, 1974) using optical methods as actinolite. The spinel is predominantly a magnesian pleonaste [$(Mg_{0.8}Fe^{2+}_{0.1}Ca_{0.04}Na_{0.06})(Al_{1.9}Fe^{3+}_{0.1})O_4$] with a minor magnetite component and trace amounts of Mn and Si. Orthopyroxene is $En_{89}Fs_{10}Wo_1$ and the olivine is very similar to the olivines found in the dunite, with an average composition of Fo_{89-90}.

Geothermometry and Geobarometry

Distribution coefficients of coexisting minerals, and ratios of the components taking part in pertinent exchange equilibria are shown in Table 4, along with various exchange equilibria and calibrations which have been used to constrain equilibration temperatures attained by the amphibolites during the prograde regional metamorphic event. Temperatures derived from these data are also presented.

Table 4. Geothermometry

Amphibolite Type	Exchange Equilibria	Sample Number	Pertinent Chemical Data for Coexisting Phases in Exchange Reaction					Temp. (°C)	Reference
	Cpx-Hbl ($Fe^{2+} \rightleftharpoons Mg$)		Al^{IV}	$(Mg/Mg + Fe^{2+})_{Cpx}$		$(Mg/Mg + Fe^{2+})_{Hbl}$	K_D		Kretz and Jen, 1978
I		6am34	1.65	0.71		0.69	1.21	750 ± 50	
I		12-1	1.50	0.73		0.65	1.46	750 ± 50	
			$(Mg/Mg + Fe^{2+} + Mn)_{Cpx}$			$(Mg/Mg + Fe^{2+} + Mn)_{Hbl}$			Perchuk, 1969
I		6am34	0.71			0.68		~720*	
I		12-1	0.71			0.64		~750*	
	Plag-Hbl ($NaSi \rightleftharpoons CaAl$)		X_{An}	Na(M4)	Ca(M4)	$\ln(X_{An}/X_{Ab})$	$\ln(Ca,M4/Na,M4)^{-}$		Spear, 1980
I		6am34	53	0.22	1.78	0.12	2.09	720 ± 25	
I		8-42	53	0.24	1.76	0.12	1.99	725 ± 25	
I		12-1	72	0.15	1.84	0.94	2.51	715 ± 25	
II		2-18	34	0.09	1.91	-0.66	3.05	520 ± 20	
II		4-10	26	0.17	1.83	-1.05	2.38	510 ± 20	
II		8-9	27	0.19	1.81	-0.99	2.25	525 ± 20	
	Gar-Hbl ($Fe^{2+} \rightleftharpoons Mg$)		$(Mg/Mg + Fe^{2+} + Mn)_{Gar}$			$(Mg/Mg + Fe^{2+} + Mn)_{Hbl}$			Perchuk, 1969
II		2-18	0.12			0.55		~440*	
	Gar-Biotite ($Fe^{2+} \rightleftharpoons Mg$)		K_D			$\ln K_D$			Thompson, 1976
		4-13	0.16			-1.83		540 ± 20	
Carolina Gneiss			$(Mg/Mg + Fe^{2+} + Mn)_{Gar}$			$(Mg/Mg + Fe^{2+} + Mn)_{Bte}$			Perchuk, 1970
		4-13	0.10			0.43		554 ± 20	
			Mg/Fe_{Gar}			Mg/Fe_{Bte}			Ferry and Spear, 1978
		4-13	0.123			0.75		527 ± 20	

*Uncertainties in method not reported in original calibration.

Temperatures calculated using the NaSi $\rightleftharpoons$ CaAl exchange equilibria between plagioclase and hornblende, empirically calibrated by Spear (1980), are based upon the variations of Na and Ca in the M4 site of amphibole, and are thus limited by the uncertainty involved in determining M4 site occupancy. Other limiting factors are the uncertainty due to plagioclase and hornblende nonideality along the exchange vector $NaSiCa_{-1}Al_{-1}$, as well as the partitioning, which is highly dependent upon mineral composition (Spear, 1980). Despite the potential flaws, this geothermometer appears to yield highly satisfactory results which are corroborated by several different Fe^{2+} - Mg exchange equilibria (e.g., Ferry and Spear, 1978; Kretz and Jen, 1978). Various calibrations of the Fe^{2+} - Mg partitioning between garnet-biotite yield similar temperatures, with those of Perchuk (1970) being somewhat high. Baltatzis (1979) has shown that variations of Ca and Mn in garnet have little or no effect on $K_{D\ gar\text{-}biot}^{Fe\text{-}Mg}$. This is supported by results from garnets analyzed in this study. Perchuk's (1969) calibration of the Fe^{2+} - Mg exchange for garnet-hornblende yields temperatures which are low by at least 70°C. Similar low results using this calibration were reported by Clague et al. (1979), who caution that temperatures obtained with this calibration may be low by as much as 65°C. The Fe^{2+} - Mg exchange for clinopyroxene-hornblende is pressure sensitive (Perchuk, 1969); therefore pressures of approximately 4-6 kb, derived from various geobarometers (see below), have been used to calculate temperature using methods described by Perchuk (1969). Kretz and Jen (1978), on the other hand, have found pressure effects to be minimal, while Al^{IV} in the

amphibole lattice causes a significant increase in K_D as the Al^{IV} content in Ca-amphibole rises. A plot of K_D versus Al^{IV} in amphiboles from Type I amphibolites falls along the granulite-facies trend outlined by Sen (1973).

Temperatures derived from various geothermometers indicate a striking difference between Type I and Type II amphibolites. Type I amphibolites display temperatures ranging from 700-750°C, clearly granulite facies conditions, while Type II amphibolites yield temperatures of approximately 510-520°C, appropriate for amphibolite facies conditions. Similar distribution coefficients and textural evidence of equilibrium suggest that these temperatures do represent at least a lower limit for equilibration temperatures attained during regional metamorphism. Fe^{2+} - Mg exchange equilibria for several garnet-biotite pairs from metasediments near the southwest contact of the amphibolite with the Carolina Gneiss yield temperatures of approximately 540 ± 20°C, which are similar to those determined for Type II amphibolites.

Pressure under which the complex has been metamorphosed has been estimated from several observations. Quantities of Al^{IV}, Al^{VI}, and Si in amphiboles are pressure sensitive, and several studies (Raase, 1974; Fleet and Barnett, 1978) have attempted to calibrate distribution of these components with increasing pressure. On an Al^{IV}-Al^{VI} plot (Figure 11a) for amphiboles (Fleet and Barnett, 1978), both Type I and Type II hornblendes from Chunky Gal Mountain plot generally within the field of low-pressure metamorphic amphiboles, although there is a good deal of scatter. Clague et al. (1981) have suggested that this scatter

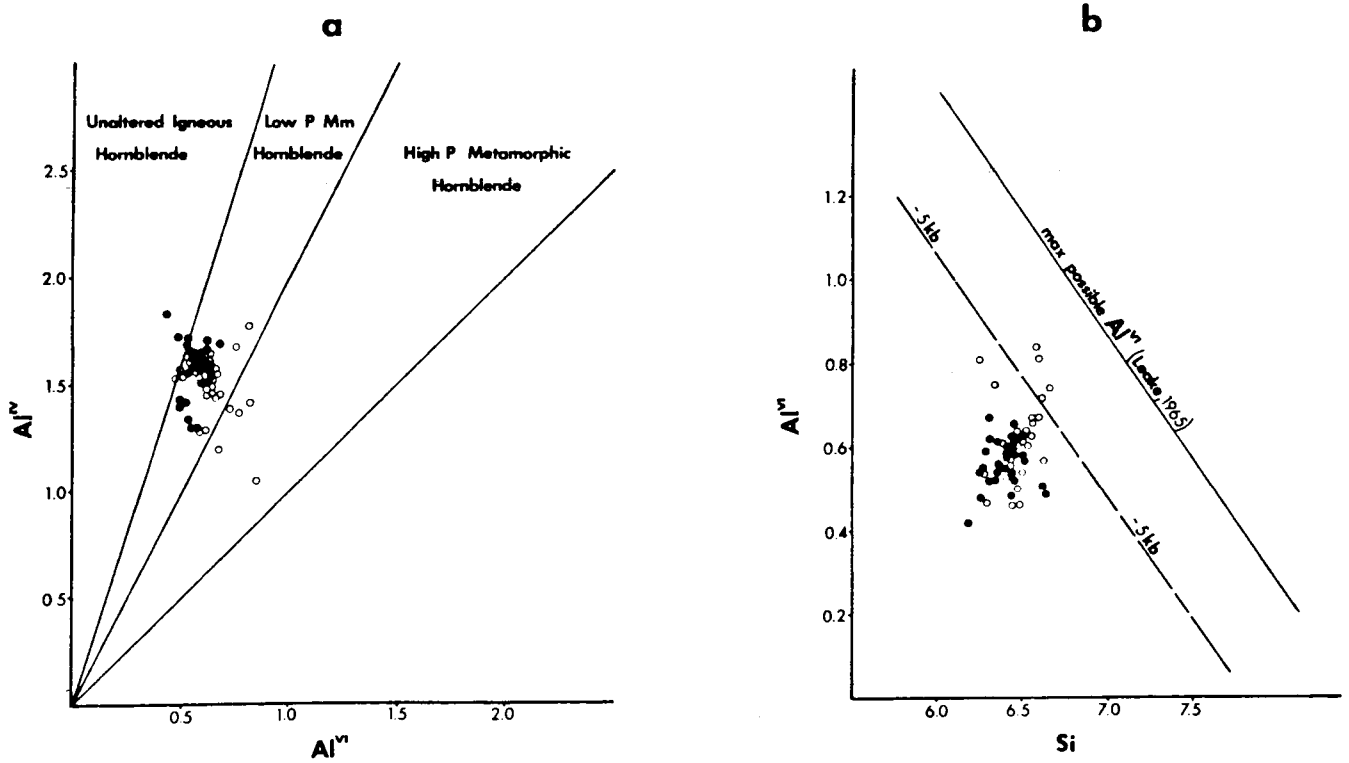

Figure 11. Variation diagrams in which Type I and Type II amphiboles are represented by filled and open circles respectively. (a) Al^{VI}-Al^{IV} diagram in cation percent, showing fields of unaltered igneous hornblende, low-pressure metamorphic hornblende, and high-pressure metamorphic hornblende (Fleet and Barnett, 1978). The line dividing the low- and high-pressure metamorphic hornblende fields represents approximatly 5 kb. (b) Si-Al^{VI} diagram (Raase, 1974) in cation percent with the dashed line representing a 5 kb boundary. Below this line pressures are 5 kb and above the line pressures are >5 kb. The solid line represents maximum possible Al^{VI} content in amphiboles at any given Si content (Leake, 1965).

may be due to variability in Fe^{3+} content of amphibole grains, since this affects Al partitioning. Because the amount of Fe^{3+} in the amphiboles has been calculated and is not actually known, this may be a significant factor in causing scatter in this diagram. A somewhat more informative diagram is Figure 11b, which is a plot of Si versus Al^{IV}. The position of the 5 kb line on this plot (Raase, 1974) suggests that this might be an upper limit to pressure experienced during metamorphism of these amphibolites. It should be noted that Type I amphiboles are in general lower in Al^{VI} and Si than Type II amphiboles although there is a large degree of overlap. Amphiboles from the Adirondacks plot within this field of overlap. Turner (1968) has postulated pressures of 3-4 kb for the formation of the Adirondack amphiboles and this estimate seems reasonable for the amphiboles at Chunky Gal Mountain.

Several reactions observed within the complex also serve to constrain the pressure estimate. Sub-solidus reaction coronas developed at plagioclase-olivine grain boundaries in the troctolite suggest minimum pressures of 5-7 kb (Gardner and Robbins, 1974); however, the presence of amphibole in the Chunky Gal Mountain coronas suggests the presence of a fluid phase which would tend to lower the pressure at which plagioclase and olivine react to form coronas (Walawender, 1976). Under water excess conditions Yoder (1965) has reported breakdown of plagioclase and olivine at pressures as low as 2 kb.

Troctolite which has been metamorphosed to amphibolite contains kyanite in some cases. Kyanite-bearing amphibolites may arise through

amphibolitization of kyanite-bearing eclogites and commonly contain hornblendes rich in the tschermakite component (Tilley, 1936a, 1936b). In many cases tschermakitic hornblende is formed by the breakdown of omphacite and garnet during retrograde metamorphism of eclogites (Deer et al., 1962). In this case though, it appears that the kyanite and hornblende, which contains an appreciable tschermakitic component, have formed as a result of progressive metamorphism of troctolite. These rocks are very aluminous and often contain corundum. The plagioclase in these amphibolites averages An_{85} as opposed to An_{95} in the troctolites. A decrease in An content from troctolite to amphibolite would release Al_2O_3 and CaO for the formation of kyanite and tschermakitic hornblende. Thus it is probable that the presence of kyanite can be used to constrain the pressure during the prograde metamorphic event. The presence of this aluminosilicate polymorph yields a lower pressure limit of 4 kb [using the aluminosilicate phase relations experimentally determined by Holdaway (1971)] when equilibration temperatures for Type II amphibolites are used, and 7 kb when the higher Type I equilibration temperatures are used. Amphiboles from the coronas in the troctolite and from the metatroctolite plot just above the 5 kb line in Figure 11b. A pressure between 4-6 kb seems reasonable when combined with other barometric indicators.

A further constraint on pressure is the observed incipient breakdown of plagioclase to scapolite. In experiments on the system Ab-An-NaCl-$CaCO_3$, Orville (1975) has shown that in the presence of $CaCO_3$, plagioclase forms scapolite at 750°C and 4 kb. This temperature has already been

established in the Type I amphibolites, and the 4 kb pressure is consistent with previous arguments. It is interesting to note that Lovering and White (1964) have suggested that sulfur-rich scapolites are characteristic of the granulite facies, and that sulfur content increases with metamorphic grade. Although minor S peaks were detected in analyzing these scapolites, the presence of carbonate near several reaction zones in these amphibolites implies that these scapolites are predominantly carbonate scapolites (Goldsmith and Newton, 1977).

CHAPTER IV

GEOCHEMISTRY

Major and selected trace element abundances and CIPW norms for twenty-three samples of amphibolite, one sample of troctolite-amphibolite, and one sample of troctolite are presented in Table 5, along with an analysis of a dunite sample from Hunter (1941). Most of the amphibolite samples are silica undersaturated and fall within the olivine tholeiite portion of the basalt tetrahedron. Several Type I amphibolites are critically undersaturated (ne-normative) and plot as alkali basalts, while several of the Type II amphibolites are oversaturated (qtz-normative) and fall within the tholeiite field. Total alkalis are low, ranging from 1% in Type I to a maximum of $\leqslant 3\%$ in Type II samples. Cluster analysis on major element chemistry of the amphibolites shows no significant separation into Type I and Type II groups; however, the same test performed on trace elements clearly differentiates between the two amphibolite types.

The possibility of sedimentary trends is tested in Figure 12, using the diagrams of Moine and LaRoche (1968), which differentiate between amphibolites with sedimentary or mafic igneous affinities (Moine and LaRoche, 1968; Moine, 1971; Bard and Moine, 1979). In both diagrams the amphibolites fall within the basaltic field and show no sedimentary trends. The amphibolites in both Figure 12a and 12b are far removed from the spilite field suggesting that they probably have not undergone ocean-floor metamorphism.

Table 5. Bulk Chemical (XRF) Analyses of Amphibolites; Major Element Oxides (Weight Percent), Trace Elements (ppm), and CIPW Norms

	1am8(I)	2am3(II)	2-18(II)	3-28(II)	3-32(II)	4-1(II)	4-10(II)	5-5(II)	5-21(II)	6am25(I)	6am34(I)	7-8(I)	8-2(II)	8-9(II)	8-15(II)	8-42(I)	9-18(I)	10-7(II)	11am9(I)	12-1(I)	12-2(I)	13-7(I)	T-7(I)	6gam36[c]	1+24B[c]	Dunite[c,d]
SiO_2	46.68	47.11	46.51	43.55	45.61	46.54	46.89	50.76	47.43	42.93	43.28	45.71	46.03	45.19	44.03	48.35	43.95	46.62	44.85	45.75	48.18	46.01	44.73	47.52	41.41	38.70
TiO_2	0.58	1.58	1.55	1.53	1.20	1.48	1.06	1.77	1.51	1.24	1.01	0.84	1.84	1.60	0.86	0.91	0.87	1.46	0.84	0.71	0.69	0.78	1.19	0.17	--	
Al_2O_3	8.48	12.27	12.57	13.19	12.55	12.47	13.47	14.48	12.03	11.85	13.61	13.21	12.85	12.61	13.31	14.63	14.51	12.62	14.26	14.64	14.31	14.01	13.30	17.77	11.58	2.52[e]
Fe_2O_3[a]	15.35	14.45	15.04	15.23	14.16	14.64	13.55	13.73	14.88	16.79	16.38	14.65	15.11	14.69	15.49	13.67	15.34	14.88	14.86	13.06	12.84	13.44	14.61	6.61	10.78	10.70
MnO	0.14	0.15	0.16	0.17	0.17	0.16	0.15	0.19	0.17	0.18	0.20	4.18	0.19	0.17	0.19	0.17	0.18	0.17	0.17	0.15	0.15	0.18	0.16	0.06	0.13	
MgO	14.24	9.03	8.17	10.54	11.24	8.66	10.72	5.62	7.37	12.26	10.68	9.43	9.13	10.11	11.06	8.97	10.07	8.93	10.65	9.36	8.98	9.94	10.31	11.37	27.7	46.52
CaO	12.05	10.85	12.07	11.26	11.09	12.96	12.12	8.99	13.42	11.86	11.51	0.18	10.51	11.03	10.84	9.54	11.83	12.30	11.44	16.32	12.24	11.48	13.07	12.63	6.93	0.56
Na_2O	0.60	1.48	0.72	1.36	1.63	1.84	2.71	2.46	1.02	0.46	0.96	9.32	1.53	1.37	1.04	1.64	0.89	1.61	1.01	1.70	0.85	1.03	1.25	1.90	1.01	
K_2O	0.32	0.23	0.29	0.49	0.26	0.22	0.22	0.22	0.16	0.39	0.12	13.63	0.36	0.35	0.34	0.20	0.16	0.28	0.24	tr	0.07	0.10	0.04	tr	--	
P_2O_5	0.12	0.11	0.12	0.10	0.10	0.13	0.11	0.15	0.13	0.09	0.09	0.51	0.12	0.11	0.09	0.10	0.10	0.12	0.10	0.12	0.11	0.10	0.11	0.11	0.05	
Rb	34.9	33.8	34.0	36.6	36.1	35.9	41.6	31.6	33.0	35.6	35.2	36.3	36.4	34.8	35.6	34.0	39.3	35.8	33.4	35.1	34.4	37.4	32.2	35.5		
Sr	33.8	112.6	225.2	108.5	120.5	232.7	140.3	179.1	176.5	43.6	46.3	31.1	119.7	137.7	52.6	115.9	64.8	178.8	49.9	75.8	43.9	78.5	112.5	160.0		
Y	33.9	22.4	25.2	18.9	20.2	23.0	15.0	33.3	20.2	23.0	20.5	18.2	26.6	21.7	20.9	19.4	21.4	19.8	18.5	13.4	16.2	15.3	17.3	4.3		
Nb	10.7	11.3	11.2	12.2	9.4	5.8	0.2	15.3	10.2	13.4	9.9	7.1	13.7	11.3	10.6	3.4	7.9	8.8	8.7	8.0	7.3	2.9	10.3	3.7		
Zr	125.2	186.7	184.1	187.2	160.0	188.5	155.9	265.6	180.8	149.8	138.5	139.1	216.0	195.2	128.7	140.7	137.9	183.7	126.7	135.3	136.2	143.7	154.6	117.8		
CIPW Norms[b]																										
Q	--	2.04	4.54	--	--	--	--	7.31	4.49	--	--	1.31	--	--	--	2.48	--	--	--	--	4.10	0.19	--	--		
Or	1.93	1.41	1.78	3.00	1.58	1.32	1.30	1.33	0.97	2.38	0.73	0.18	2.20	2.15	2.09	1.22	0.98	1.69	1.46	--	0.42	0.61	0.24	--		
Ab	5.19	13.00	6.33	11.93	14.20	15.86	18.29	21.36	8.88	4.01	8.39	4.44	13.39	12.04	9.14	14.27	7.77	13.89	8.77	7.41	7.37	9.06	10.81	16.44		
An	19.94	27.16	31.39	29.49	26.94	25.58	23.90	28.55	28.58	30.03	33.56	34.62	28.07	28.28	31.84	32.86	36.23	26.90	34.55	31.99	35.89	34.62	31.24	40.87		
Ne	--	--	--	--	--	--	2.49	--	--	--	--	--	--	--	--	--	--	--	--	3.70	--	--	--	--		
Di	32.53	22.72	24.54	22.50	23.48	31.83	28.67	13.38	31.98	24.35	20.22	27.81	20.37	22.56	19.03	12.33	19.25	28.13	18.69	38.44	20.80	19.40	27.81	17.93		
Hy	25.87	23.91	21.43	8.28	13.61	9.72	--	18.32	15.34	16.48	16.06	23.34	25.43	19.88	18.22	28.87	18.95	16.55	20.03	--	24.22	28.38	10.41	7.97		
Ol	6.12	--	--	14.83	11.40	6.19	17.32	--	--	12.74	11.64	--	0.02	5.19	10.93	--	8.10	3.27	8.14	11.33	--	--	10.57	13.25		
Mt	6.60	6.31	6.57	6.65	6.14	6.28	5.69	5.92	6.44	7.28	7.12	6.34	6.57	6.42	6.76	5.90	6.66	6.39	6.41	5.44	5.53	5.88	6.28	2.85		
Il	1.13	3.12	3.06	3.01	2.35	2.86	2.01	3.45	2.95	2.43	1.98	1.64	3.61	3.16	1.70	1.78	1.70	2.83	1.64	1.34	1.34	1.54	2.31	0.33		
Ap	0.29	0.27	0.30	0.25	0.24	0.31	0.26	0.36	0.32	0.22	0.22	0.27	0.29	0.27	0.22	0.24	0.24	0.29	0.24	0.28	0.27	0.25	0.27	0.27		

[a] All Fe calculated as Fe_2O_3.

[b] All norms calculated with an assumed Fe^{2+}/Fe^{3+} ratio of 2.5.

[c] Ultramafic lithologies 6gam36, 1+24B, Dunite represent Troctolite-Amphibolite, Troctolite, and Dunite, respectively.

[d] Dunite analysis from Hunter (1941).

[e] TiO_2, Cr_2O_3, and Al_2O_3 combined.

[f] 1am8(I) sample number; roman numeral in parenthesis indicates Type I or II amphibolite.

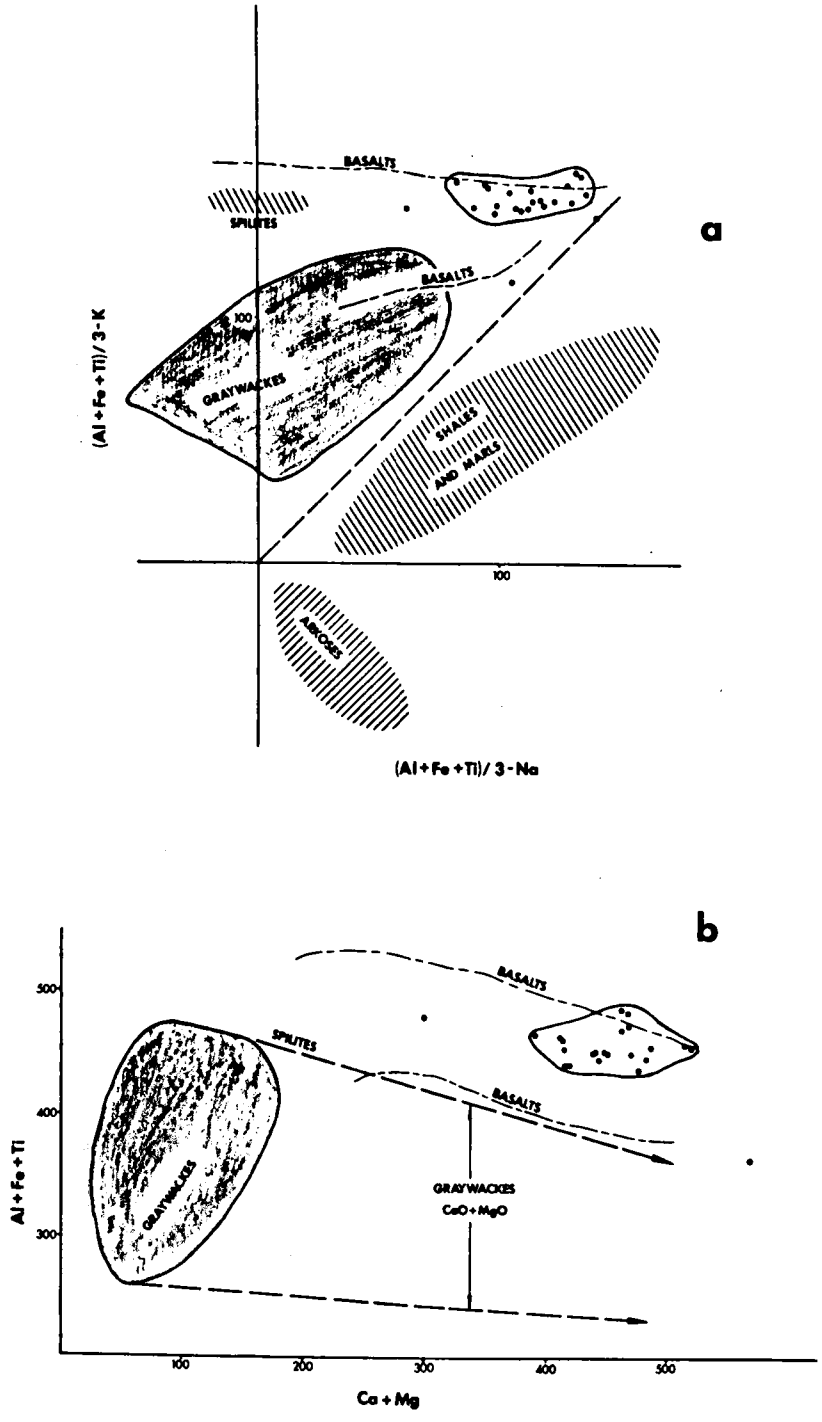

Figure 12. Filled circles represent Chunky Gal Mountain amphibolites in these diagrams showing discrimination between basaltic and sedimentary compositions (Moine et al., 1968). Al, Fe, . . . etc., are the contents in millimoles of each element in 100 gm of rock. (a) (Al + Fe + Ti)/3-K versus (Al + Fe + Ti)/3-Na. (b) Al + Fe + Ti versus Ca + Mg.

It is apparent from variation diagrams (Figure 13) that both Type I and Type II amphibolites lie along the same differentiation trend. The amphibolites do not show a strong iron enrichment trend with progressive differentiation, possibly indicating a high fO_2 during igneous crystallization. The MgO content in the amphibolites decreases, while TiO_2 increases with an increase in mafic index (Figure 13). These trends must reflect differentiation and suggest that even when subjected to high-grade metamorphism, these elements remain relatively immobile. The same can be said for Y and Zr (Figure 13), which makes the use of tectonic discriminant diagrams employing these elements (e.g., Pearce and Cann, 1973), an attractive possibility. It thus appears that much of the chemical variation observed within the Chunky Gal Mountain amphibolites can be ascribed to early magmatic differentiation.

All of the Chunky Gal Mountain amphibolites have low K_2O, Na_2O and BaO contents, with the alkali contents increasing slightly with mafic index; however, there is a great deal of scatter which suggests significant alkali metasomatism (Figure 13). The effects of metasomatism are also suggested in the Ti/100-Zr-Sr/2 ternary discriminant diagram (Figure 14a) of Pearce and Cann (1973). Both Type I and Type II amphibolites are scattered and trend away from the Sr/2 apex. With this caution in mind, Figure 14a may still be used to suggest a tectonic setting for the amphibolites. Both Zr and Ti appear to have been relatively immobile and Sr appears to have been depleted. Extrapolating back toward the Sr/2 apex we see that both Type I and Type II rocks show calc-alkaline affinities. This setting is supported by another Pearce

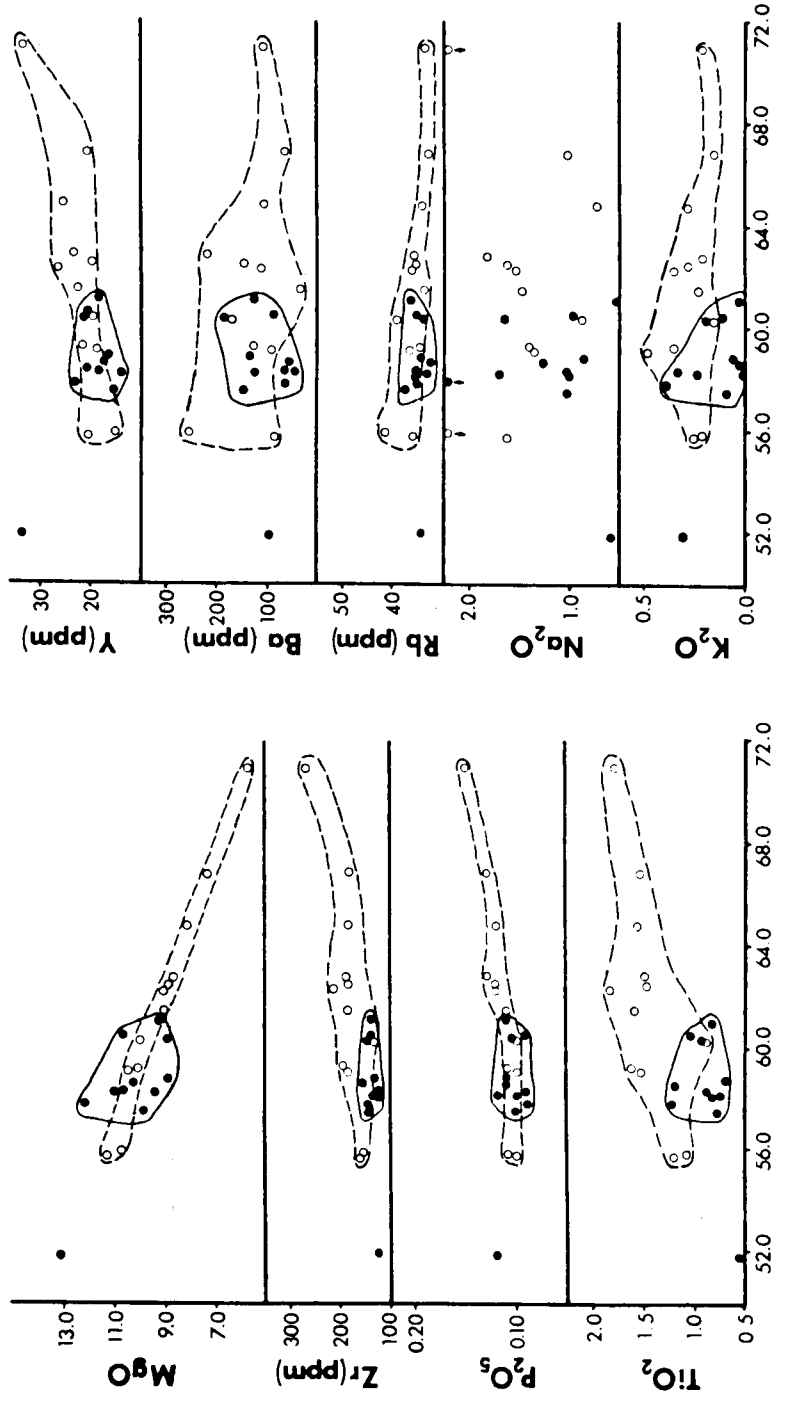

Figure 13. Selected major element oxides (weight percent) and trace elements (ppm) plotted against the mafic index (100 × Fe_2O_3(t)/Fe_2O_3(t) + MgO). Fe_2O_3(t) is total iron as Fe_2O_3. Filled circles represent Type I and open circles represent Type II amphibolites respectively. One Type I amphibolite analysis, excluded from the circled cluster appears to be anamalous in its chemical and mineralogic properties.

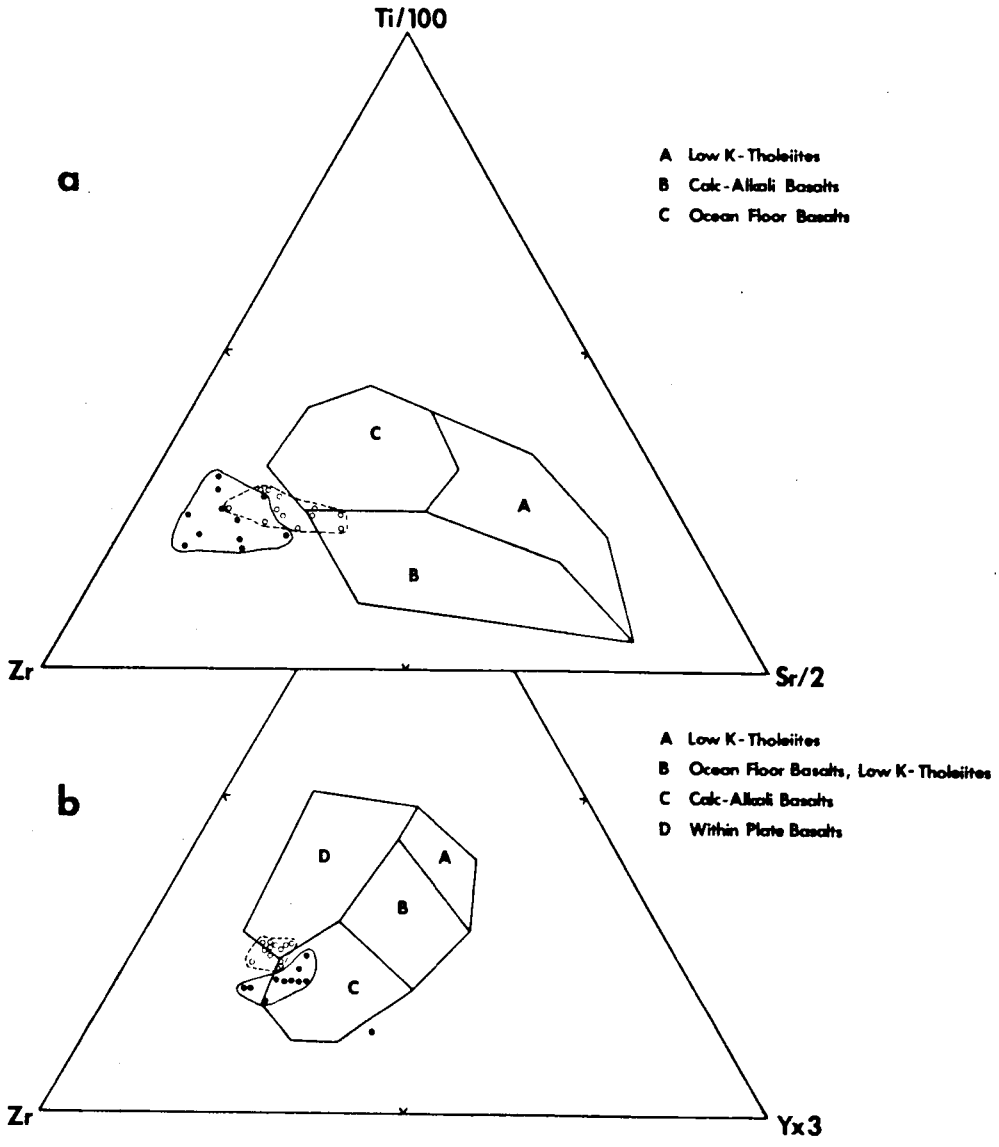

Figure 14. Ternary discrimination diagrams of Pearce and Cann (1973). Units are ppm and filled circles represent Type I amphibolites, while open circles represent Type II amphibolites. (a) Ti/100-Zr-Sr/2. (b) Ti/100-Zr-Yx3.

and Cann (1973) diagram (Figure 14b) in which the amphibolites plot predominantly in the calc-alkaline field. Again there is a distinct segregation with only minor overlap between Type I and Type II amphibolites. Type II rocks straddle the boundary between the calc-alkaline and within-plate basaltic rocks in Figure 14b, which may be a function of increasing relative Ti content with differentiation.

The major element discriminant diagrams of Pearce (1976) may be used in a circuitous fashion to constrain the protolith. Of the twenty-three amphibolite samples, nineteen did not meet the screen of $12\% < CaO + MgO < 20\%$. (CaO + MgO) behaves as a simple fractionation index and the range of values for this index, as stipulated by Pearce (1976), was chosen to cover those rocks which are conventionally termed basalts. Most of the amphibolite samples do not meet the screen because (1) the major element chemistry is such that these rocks are probably not metabasalts, or (2) there has been significant mobility of these components under open system conditions allowing CaO and/or MgO to be either enriched or depleted. The apparent igneous differentation trends shown by these components appear to discount the second suggestion. (CaO + MgO), in all cases where the screen is not met, is higher than 20% suggesting that the amphibolites may well have been derived from mafic cumulate rocks. This observation may explain some of the peculiarities in the previous discriminant plots, which were derived using basaltic liquid compositions.

CHAPTER V

PETROGENESIS

Amphibolite Protolith

One important aspect of the petrogenesis of this complex is the identification of the amphibolite protolith. Several lines of evidence support an igneous origin and further suggest that the precursor may have been a gabbroic cumulate. Compositional differences from para-amphibolites (Figure 12), the lack of interbedded metasedimentary rocks, and a general absence of calcite and presence of only minor quartz in mafic assemblages support an igneous origin. The amphibolites also exhibit igneous differentiation trends (Figure 13) in those components which are immobile during subsequent metamorphism. The majority do not meet the screen of $12\% < CaO + MgO < 20\%$, which was chosen by Pearce (1976) to cover the range of rocks normally classed as basalts. Screen values greater than 20% in these amphibolites suggest that the protoliths may have been rich in cumulate phases, and hence do not represent liquid compositions. To the extent that tectonic discriminant diagrams of Pearce and Cann (1973) can be used for cumulate rocks, these diagrams suggest calc-alkaline affinities for these amphibolites.

Metamorphism

Regional metamorphism of this complex has produced two distinct mafic assemblages designated as Type I and Type II amphibolites.

Temperature estimates obtained with various geothermometers range from 700-750 ± 50°C for Type I and 510-520 ± 25°C for Type II amphibolites, while P_{total} has been constrained to approximately 4-6 kb for the entire complex. Minor bulk chemical differences in ACF components between Type I and Type II amphibolites (Figure 15) were not sufficient to affect noticeably the appearance of specific minerals, but may have caused modal variations. This has also been shown to be the case by Glassley and Sørenson (1978) for metadolerites of similar composition. It is much more likely that the differences between Type I and Type II assemblages are brought about by variations in temperature, X_{H_2O} in the fluid phase, and oxygen fugacity. Phillips (1980), studying changes in a_{H_2O} across an amphibolite-granulite transition in Australia, found that a_{H_2O} tends to decrease significantly across the transition zone in the up-grade direction, but that temperature was the more important factor in accounting for the higher grade assemblages. Differences in X_{H_2O} appear to characterize Type I and Type II amphibolites in the Chunky Gal Mountain complex. Energy dispersive analyses have shown that H_2O appears to be the only volatile constituent in the amphiboles of both Type I and Type II amphibolites. As metamorphic grade increases, modal hornblende diminishes and those amphiboles which remain tend to be typically hydroxyl-deficient and brownish, similar to the brown hornblende observed by Engel and Engel (1964) in Adirondack granulites. As X_{H_2O} in the fluid phase decreases there is an increase in the mole fraction of other volatile constituents such as CO_2 (and possibly S and Cl), as suggested by the prograde breakdown of plagioclase to carbonate-scapolite and the

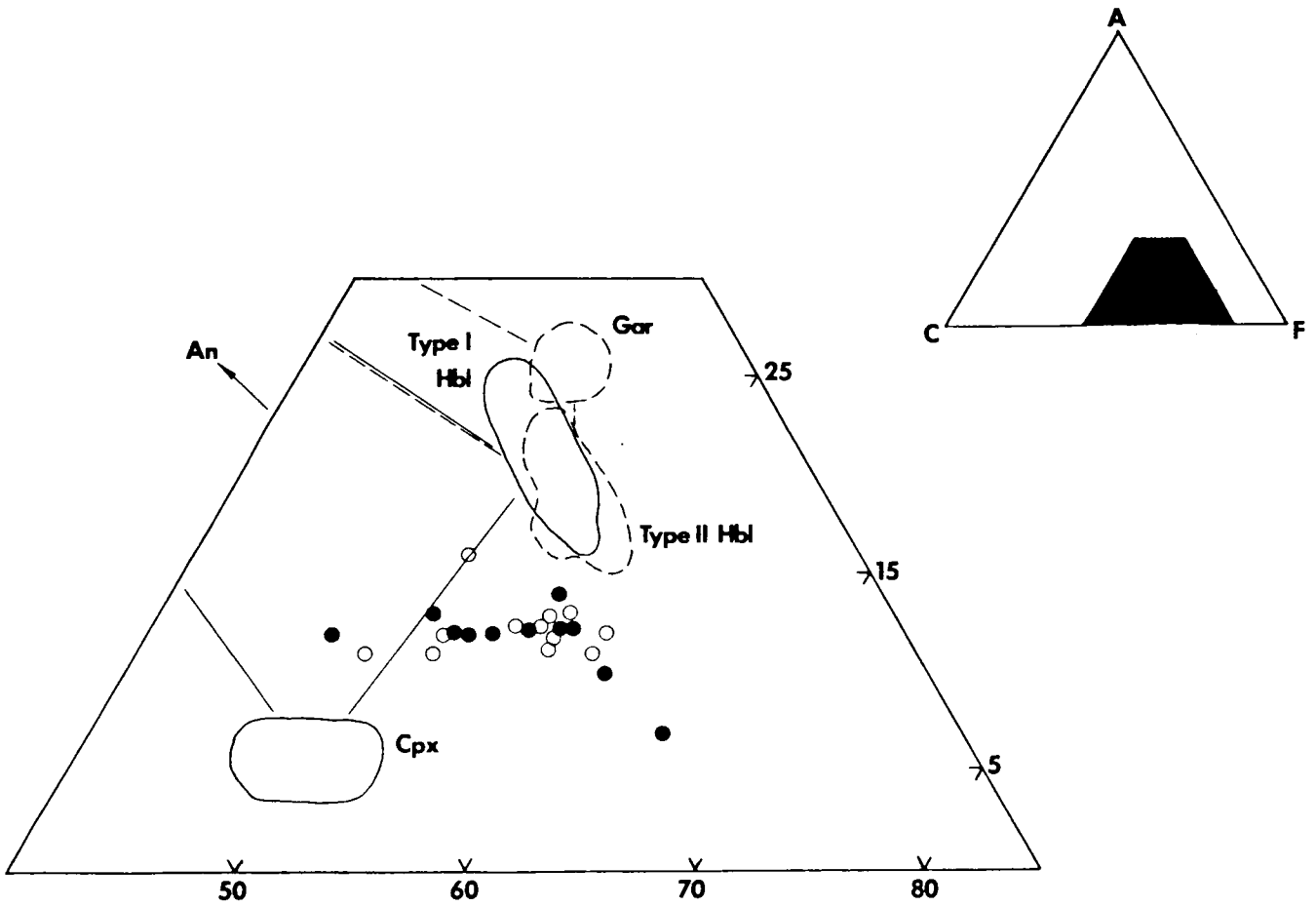

Figure 15. ACF diagram showing whole-rock compositions of Type I (filled circles) and Type II (open circles) amphibolites, respectively. Mineral compositions are those in Figure 4, p. 18 (solid lines represent Type I assemblages and dashed lines represent Type II assemblages). The open bar labelled An represents the An content of plagioclase as plotted on the A-C join. An assumed Fe^{2+}/Fe^{3+} ratio of 0.71 was used for all samples (see Field Methods and Analytical Techniques).

presence of accessory calcite in Type I rocks. At the temperatures, pressures, and inferred fluid compositions described for Type I rocks, scapolite is the stable phase relative to plagioclase (Orville, 1975; Goldsmith and Newton, 1977). The distribution of this reaction is patchy and minor where observed, which suggests that even though the fluid phase is enriched in volatiles other than H_2O, the activities of these components were not high enough to drive the plagioclase-scapolite reaction to completion. If $P_{fluid} < P_{total}$, a common condition in granulites (Winkler, 1979), the loss of a large portion of the fluid phase may have caused intergranular channels to be occluded and a granoblastic texture to dominate in Type I rocks. This may account for the haphazard retrograde effects observed within Type I rocks, while the well-foliated Type II rocks show much more widespread diapthoritic effects.

Another parameter which varies from Type I to Type II rocks is oxygen fugacity. Spear (1976) synthesized amphiboles from a basaltic starting composition at P_{fluid} = 3 kb on the WM, QFM, and HM buffers. He reported Fe^{3+} contents (as a percentage of total Fe) of 11.4 ± 1%, 12.5 ± 1%, and 40.0 ± 4% for the amphiboles synthesized on the respective buffers. Although individual values are varied, calculated Fe^{3+} values (as percent of total Fe) for Type II amphiboles average 14.3%, suggesting oxygen fugacities approximate to the QFM buffer, whereas the Fe^{3+} values for Type I amphiboles average 45.5% suggesting oxygen fugacities approximate to the HM buffer. The oxide assemblage of magnetite-ilmenohematite-hemoilmenite (Figure 10, p. 36) present in

Type I rocks may also suggest that fO_2 was buffered along HM. Assuming these buffers were operable and using the temperatures derived earlier, estimated values of fO_2 for Type I and Type II amphibolites are approximately 3.2×10^{-12} atm and 1.6×10^{-24} atm, respectively. Aside from the obvious effects on the Fe^{2+}/Fe^{3+} ratio, higher fO_2 values tend to increase Si and decrease Al, Ti, and Na in hornblendes, whereas higher temperatures have the opposite effect on these components (Spear, 1976). Inspection of the relative concentrations of these components in Type I and Type II amphibolites, however, indicates that temperature was the dominant factor controlling the incorporation of these minor elements in amphibole, while the role of increasing fO_2 may have been to decrease the rate of change of incorporation of these elements. Thus it appears that no one parameter is solely responsible for the mineralogical changes observed from Type I to Type II amphibolites, but rather these changes are a manifestation of a complex interplay between decreasing fO_2, increasing X_{H_2O} in the fluid phase, and decreasing temperature.

A retrograde event of middle greenschist facies has produced an actinolite-chlorite-epidote assemblage as well as symplectites of quartz and epidote after plagioclase. The effects of this event are very patchy in Type I amphibolites and somewhat more widespread within Type II amphibolites. Serpentinization of ultramafic rocks probably occurred at this time.

Relationships between Metamorphism and Tectonism

Table 6, modified from Hatcher and Butler (1979), summarizes the regional kinematic sequence of the southern Appalachian Blue Ridge and Piedmont and the relation of these events to the deformation and petrogenesis of the Chunky Gal Mountain complex. The first event which affected the complex was the development of the mafic-ultramafic association, either as interlayered units within an igneous protolith, or by diapiric intrusion of the ultramafic rocks into the amphibolite precursor. The first fold system (F_2) observed at Chunky Gal Mountain is an isoclinal recumbent system which produced an axial planar penetrative fabric (S_2). This fabric developed simultaneously with the prograde metamorphic event (M_1) as previously described. As temperature decreased the Chunky Gal Mountain thrust fault (Hatcher and Butler, 1979) was activated, resulting in the emplacement of the complex to its present position. The fault truncates the axial planar foliation. A retrograde event of middle- to upper-greenschist facies affected the rocks of the Chunky Gal Mountain complex prior to, or during F_3 deformation. The last fold event documented at Chunky Gal Mountain is a crenulation (F_4) which is poorly developed and does not show a penetrative fabric. Many late-stage brittle fractures and faults occur within the amphibolite and are probably related to the Alleghanian orogeny. The fractures are mineralized and contain quartz, calcite, albite, and later void-filling chlorite. They commonly contain breccia fragments of amphibolite which can be seen altering to greenschist.

Table 6. Structural Elements, and Deformational and Metamorphic Events in the Southern Appalachian Blue Ridge and Western Piedmont Modified from Hatcher and Butler (1979)

Metamorphism		Folds			Lineations				
Generation	Grade	Generation	Style	Orientation/Vergence	Generation	Type	Faults	Timing	Remarks
		F_6	Upright open	NW				Alleghanian?	
		F_5	Upright open	NE NW Vergent			Brevard (Brittle Phase) Great Smoky	Alleghanian	Mineralization of faults and fractures*
		F_4	Crenulation Cleavage*	NE NW and/or SE Vergent	L_4	Crenulation*			Not well-developed at Chunky Gal Mountain
							Linville Falls	Acadian	
M_2	Middle Greenshist*	F_3	Upright Isoclinal to open (ductile)*	NE NW Vergent	L_3	Intersection*	Inner Piedmont Nappes	Late Taconic	
		F_2	Isoclinal Recumbent*	EW to NE N to NW Vergent	L_2	Elongation*	Brevard, Chunky Gal*	Taconic	Dominant S-surface
M_1	Amphibolite to Granulite*	F_1	Isoclinal Recumbent	EW to NE N to NW Vergent	L_1	Elongation	Hayesville, Shope Fork, Greenbriar, Brevard	Taconic	S_1 rarely observed, commonly transposed

*Observed at Chunky Gal Mountain.

Two Models for the Origin of the Complex

Evidence presented above indicates an igneous protolith for the amphibolites and suggests that they were derived from gabbroic cumulates. Along with the ultramafic rocks of the complex, the amphibolites lie along the CaO-MgO-Al_2O_3 ternary differentiation trend commonly observed in ophiolite cumulate sequences (Coleman, 1977). Most of the lithologies normally found in the basal portions of ophiolites are found at Chunky Gal Mountain, assuming the amphibolites do actually represent mafic cumulates. However, detailed structural study is required to determine if the map patterns of this complex represent folded ophiolite stratigraphy rather than infolded ultramafic diapirs. If Type I and Type II amphibolites are joined along an undisturbed isograd, then metamorphism under a high geothermal gradient would have produced the different metamorphic assemblages. Such an isograd contact is suggested by a lack of field evidence for a faulted contact and by several samples near the contact which possess features common to both Types I and II amphibolites. Several previously described ophiolitic amphibolite-ultramafic associations (Coleman, 1970; Shiraki, 1971; Pamić et al., 1973) have been subjected to dynamothermal metamorphism in high heat flow regimes such as are developed in island-arc or continental margin settings. A striking analogy is the well documented ophiolite from the Darval Bay-Lubuk-Palawan region of North Borneo and the Phillippines (Hutchison, 1975). This ophiolite has developed a strong dynamothermal metamorphic fabric, and within 1 km the basal sequence changes from tectonized peridotite (mainly dunite and peridotite) through hornblende

granulite to garnet amphibolite. The same metamorphic units are observed on the same scale at Chunky Gal Mountain, although the stratigraphy is not readily apparent.

An alternative possibility is that the amphibolites represent intrusive equivalents of the meta-volcanic rocks which are intercalated with sediments found elsewhere in the Blue Ridge. These intrusive rocks may have been intruded later by ultramafic diapirs. The silica undersaturated nature of the amphibolites is consistent with a continental rifted environment such as that proposed by Hatcher (1978). Shaw et al. (1981) have examined Nd-Sm and Rb-Sr systematics in modern oceanic crust and have compared this data to isotopic data from the Thetford Mines complex, Quebec, and the Baltimore Mafic complex, Maryland. They have concluded that the mafic-ultramafic bodies of the Appalachians south of Newfoundland are not pieces of oceanic crust, but may have continental affinities.

Based on the evidence presented, neither model is unequivocally supported. The tectonic setting (island arc or continental margin), inferred from trace element discriminant diagrams, is not strongly suggestive of either, although mid-ocean ridges are not the only tectonic setting for ophiolite generation (Coleman, 1977). For example, ophiolites formed in back-arc basins (e.g., Bakor et al., 1976) are chemically similar to the Chunky Gal Mountain complex and may have calc-alkaline affinities. The effects of crustal contamination or partial melting at high pressures in the rifted continental model may yield similar results.

Each model has implications for emplacement of the Buck Creek ultramafic. In the dismembered ophiolite model, the ultramafic body represents part of the basal section of an ophiolite which was metamorphosed, deformed and thrusted to its present position together with its associated mafic rocks. In the rifted continent model, the amphibolites represent the intrusive equivalents of undersaturated basalts emplaced into the accumulated sedimentary pile. They may have been subsequently intruded diapirically by ultramafics, possibly the residues from partial melting. After ultramafic intrusion the entire complex was metamorphosed, deformed and tectonically emplaced to its present position.

Petrofabric studies of Sailor and Kuntz (1973) suggested that the dominant fabric and texture of the dunite were developed by recrystallization in the upper mantle, since the mineral fabric is not concordant with the regional S_2 foliation. This does not rule out either of the two major hypotheses (dismembered ophiolite or diapiric intrusive) concerning the origin of the ultramafic rocks. However, neither model can explain why the dunite has not recrystallized along with the amphibolite during M_1 metamorphism. Troctolites closely associated with the dunite grade into troctolite-amphibolites with an S_2 foliation, arguing against emplacement of the ultramafic body after M_1. Brittle deformation features superimposed on mantle derived textures occurred after emplacement of the entire complex. The cataclasis observed in the amphibolite, which is localized along certain areas of the mafic-ultramafic contact, may have been cuased by differential movement

either during emplacement of the entire complex or during subsequent deformation. Alternatively it may have been caused by emplacement of the ultramafic body along a faulted contact. However, the cataclastic zone is formed in amphibolite, not gabbro, and shows no signs of recrystallization as would be expected if the dunite were tectonically emplaced into the mafic rocks prior to M_1 metamorphism.

The complex history of the Buck Creek ultramafic body has so far precluded a determination of its mechanism of emplacement. Unfortunately, the origin of its associated mafic rocks is equally problematic, and does not yield a mechanism which can unequivocally explain the origin of the ultramafic rocks.

REFERENCES

REFERENCES

Albee, A. L., and Ray, L., 1970, Correction factors for electron probe microanalysis of silicates, oxides, carbonates, phosphates, and sulfates: Anal. Chem., v. 42, p. 1408-1414.

Allison, I., and LaTour, T., 1977, Brittle deformation of hornblende in a mylonite: A direct geometrical analogue of ductile deformation by translation gliding: Can. Jour. Earth Sciences, v. 14, n. 8, p. 1953-1958.

Bakor, A. R., Goss, I. G., and Neary, C. R., 1976, Jabal al Wask, northwest Saudi Arabia: An Eocambrian backarc ophiolite: EPSL, v. 30, p. 1-9.

Baltatzis, E., 1979, Distribution of Fe and Mg between garnet and biotite in Scottish Barrovian metamorphic zones: Mineral. Mag., v. 43, p. 155-157.

Bard, J. P., and Moine, B., 1979, Acebuches amphibolites in the Aracena Hercynian metamorphic belt (Southwest Spain); geochemical variations and basaltic affinities: Lithos, v. 12, n. 4, p. 271-282.

Barr, A. J., Goodnight, J. H., Sall, J. P., Blair, W. H., and Chilko, D. M., 1979, SAS Users Guide: SAS Institute Inc., 494 p.

Bence, A. E., and Albee, A. L., 1968, Empirical correction factors for the electron microanalysis of silicates and oxides: Jour. Geology, v. 76, p. 382-403.

Brobst, D. A., 1962, Geology of the Spruce Pine District, Avery, Mitchell, and Yancey Counties, North Carolina: U.S. Geol. Survey Bull., v. 1122-A, 26 p.

Chidester, A. H., and Cady, W. M., 1972, Origin and emplacement of alpine-type ultramafic rocks: Nature Phys. Sci., v. 240, p. 27-31.

Clague, D., Rubin, J., and Brackett, R., 1981, The age and origin of the garnet amphibolite underlying the Thetford Mines ophiolite, Quebec: Can. Jour. Earth Sciences, v. 18, n. 3, p. 469-486.

Coleman, P. J., 1970, Geology of the Soloman and New Hebrides Islands, as part of the Melanesian re-entrant, Southwest Pacific: Pacific Sci., v. 24, p. 289-314.

Coleman, R. G., 1977, Ophiolites: Springer-Verlag, New York, 229 p.

Deer, W. A., Howie, R. A., and Zussman, J., 1962, Rock-forming minerals, v. 2 chain silicates: Longman, Green, and Co. Ltd., London, 379 p.

_____, 1978, Rock-forming minerals: Single chain silicates; 2nd ed., New York, John Wiley and Sons, 668 p.

Dougan, T. W., 1974, Cordierite gneisses and associated lithologies of the Guri area, Northwest Guayana Shield, Venezuela: Contr. Mineralogy and Petrology, v. 46, p. 169-188.

Engel, A. E. J., and Engel, C. E., 1962b, Hornblendes formed during progressive metamorphism of amphibolite, northwest Adirondack mountains, New York: Geol. Soc. America Bull., v. 73, p. 1499-1514.

_____, and Havens, R. G., 1964, Mineralogy of amphibolite interlayers in the gneiss complex, northwest Adirondack mountains, New York: Jour. Geology, v. 72, p. 131-156.

Evans, B. W., and Leake, B. E., 1960, The composition and origin of the striped amphibolites of Connemara, Ireland: Jour. Petrology, v. 1, p. 337-363.

Ferry, J. M., and Spear, F. S., 1978, Experimental calibration of the partitioning of Fe and Mg between biotite and garnet: Contr. Mineralogy and Petrology, v. 66, p. 113-117.

Flanagan, F. J., 1969, U.S. Geological Survey standards—II. First compilation of data for the new U.S.G.S. rocks: Geochim. et Cosmochim. Acta, v. 33, p. 81-120.

_____, 1976, Descriptions and analyses of eight new U.S.G.S. rock standards: U.S. Geol. Survey Prof. paper 840, 192 p.

Fleet, M. E., and Barnett, R. L., 1978, Al^{IV}/Al^{VI} partitioning in calciferous amphiboles from the Frood Mine, Sudbury, Ontario: Can. Mineralogist, v. 16, p. 527-532.

Gardner, P. M., and Robins, B., 1974, The olivine-plagioclase reaction: geological evidence from the Seiland petrographic province, northern Norway: Contr. Mineralogy and Petrology, v. 44, p. 149-156.

Glassley, W. E., and Sørensen, K., 1980, Constant P_S-T amphibolite to granulite facies transition in Agto (West Greenland) metadolerites: Implications and applications: Jour. Petrology, v. 21, p. 69-105.

Goldsmith, J. R., and Newton, R. C., 1977, Scapolite-plagioclase stability relations at high pressures and temperature in the system $NaAlSi_3O_8$-$CaAl_2Si_2O_8$-$CaCO_3$-$CaSO_4$: Am. Mineralogist, v. 62, p. 1063-1081.

Gomes, C., deB., Santini, P., and Dutra, C. V., 1964, Petrochemistry of a Precambrian amphibolite from the Jaraguá area, São Paulo, Brazil: Jour. Geology, v. 72, p. 664-680.

Griggs, D. T., Turner, F. J., and Heard, H. C., 1958, Deformation of rocks at 500°C to 800°C, in Rock deformation, Griggs, D., and Handin, J., eds.: Geol. Soc. America Mem. 79, p. 39-104.

Hadley, J. B., 1949, Preliminary report on corundum deposits in the Buck Creek peridotite, Clay County, North Carolina: U.S. Geol. Survey Bull., v. 948-E, 25 p.

_____, 1970, The Ocoee Series and its possible correlatives, in Studies of Appalachian geology—central and southern, Fisher, G. W., and others, eds.: New York, Interscience Publishers, p. 247-259.

Hartley, M. E., III, 1973, Ultramafic and related rocks in the vicinity of Lake Chatuge: Georgia Geol. Survey Bull., v. 85, 61 p.

_____, and Penley, H. M., 1974, The Lake Chatuge sill outlining the Brasstown antiform: Georgia Dept. Nat. Res., Geol. Survey Georgia, Guidebook 13, 27 p.

Hasler, M. R., and Kemp, J. W., 1957, American Soc. for Testing Material, A.S.T.M. Committee E-2, Philadelphia.

Hatcher, R. D., Jr., 1978, Tectonics of the western Piedmont and Blue Ridge, southern Appalachians: Review and Speculation: Am. Jour. Sci., v. 278, p. 276-304.

_____, and Butler, J. R., 1979, Guidebook for southern Appalachian field trip in the Carolinas, Tennessee, and northeastern Georgia: Inter. Geol. Correl. Prog.—Caledonide Orogen Prog. 27 Fieldtrip guidebook, 117 p.

Higgins, M. W., 1971, Cataclastic rocks: U.S.G.S. Prof. Paper 687, 97 p.

Holdaway, M. J., 1971, Stability of andalusite and the aluminum silicate phase diagram: Am. Jour. Sci., v. 271, p. 97-131.

Hopkins, O. B., 1914, Asbestos, talc, and soapstone deposits of Georgia: Georgia Geol. Survey Bull., v. 29, 319 p.

Hunter, C. E., 1941, Forsterite olivine deposits of North Carolina and Georgia: North Carolina Dept. of Cons. and Devel., Div. of Min. Res. Bull. 41, 117 p.

Hurst, V. J., 1955, New evidence of volcanism in Georgia [abs.]: Georgia Acad. Sci. Bull., v. 13, p. 57.

Hurst, V. J., 1973, Geology of the southern Blue Ridge belt: Am. Jour. Sci., v. 273, p. 643-670.

_____, and Jones, L. M., 1973, Origin of amphibolites in the Cartersville-Villa Rica area, Georgia: Geol. Soc. America Bull., v. 84, p. 905-912.

Hutchison, C. S., 1975, Ophiolite in southeast Asia: Geol. Soc. America Bull., v. 86, p. 797-806.

Kretz, R., and Jen, L. S., 1978, Effect of temperature on the distribution of Mg and Fe^{2+} between calcic pyroxene and hornblende: Can. Mineralogist, v. 16, p. 533-537.

Kuntz, M. A., 1964, Compositional, mineralogical, and textural variation in the Buck Creek dunite, Clay County, North Carolina: unpublished M.S. thesis, Northwestern University.

Laird, J., and Albee, A. L., 1981, Pressure, temperature, and time indicators in mafic schist: Their application to reconstructing the polymetamorphic history of Vermont: Am. Jour. Sci., v. 281, p. 127-175.

Leake, B. E., 1978, Nomenclature of amphiboles: Am. Mineralogist, v. 63, p. 1023-1052.

Lovering, J. F., and White, A. J. R., 1964, The significance of primary scapolite in granulitic inclusions from deep-seated pipes: Jour. Petrology, v. 5, p. 195-218.

McElhaney, M. S., and McSween, H. Y., Jr., 1981, Is there a common origin for the mafic and ultramafic rocks of the Chunky Gal Mountain complex, North Carolina? [abs.]: Geol. Soc. America Abs. with Programs, v. 13, p. 30.

Mehta, P. K., 1976, Geochemistry and origin of the amphibolites of Kulu, NW Himalaya, India: Neues, Jahrb. Miner., Mh., v. 8, p. 365-378.

Mevel, C., Caby, R., and Kienast, J.-R., 1978, Amphibolite facies conditions in the oceanic crust: Example of amphibolitized flaser-gabbro and amphibolites from the Chenaillet ophiolite massif (Hautes Alpes, France): EPSL, v. 39, p. 98-108.

Misra, K. C., and Keller, F. B., 1978, Ultramafic bodies in the southern Appalachians: A review: Am. Jour. Sci., v. 278, p. 389-411.

Moine, B., 1971, Caractères de sédimentation et de métamorphisme des séries précambriennes épizonales à catazonales du Centre de Madagascar (région d'Ampbatofinandrahana). Approche structurale, pétrographique et spécialment géochemique: Thèse Nancy 20 octobre 1971, Sci. de la Terre, 1974, mémoire n° 31, 293 p.

Moine, B., and LaRoche, H. (de), 1968, Nouvelle approche du problème de l'origine des amphibolites à partir de leur composition chimique: C. R. Acad. Sci. Paris, v. 267D, p. 2084-2087.

Orville, P. M., 1975, Stability of scapolite in the system Ab-An-NaCl-$CaCO_3$ at 4 kb and 750°C: Geochim. et Cosmochim. Acta, v. 39, p. 1091-1105.

Pamić, J., Scavnicar, S., and Medjimorec, S., 1973, Mineral assemblages of amphibolites associated with alpine-type ultramafics in the Dinaride ophiolite zone (Yugoslavia): Jour. Petrology, v. 14, p. 133-157.

Parker, J. M., III, 1952, Geology and structure of part of the Spruce Pine District, North Carolina: North Carolina Div. Min. Res. Bull., v. 65, 26 p.

Pearce, J. A., 1976, Statistical analysis of major element patterns in basalts: Jour. Petrology, v. 17, p. 15-43.

_____, and Cann, J. R., 1973, Tectonic setting of basic volcanic rocks determined using trace element analysis: EPSL, v. 19, p. 290-300.

Perchuk, L. L., 1969, The effect of temperature and pressure on the equilibration of natural iron-magnesium minerals: Inter. Geology Review, v. 11, p. 875-901.

_____, 1970, Equilibrium of biotite with garnet in metamorphic rocks: Geochem. Inter., p. 157-179.

Perry, K., 1967, Methods of petrologic calculation and the relationship between mineral and bulk chemical composition: Wyoming Univ. Contr. Geology, v. 6, p. 5-38.

_____, 1969, A computer program which computes the mode: Wyoming Univ. Contr. Geology, v. 8, p. 9-18.

Petty, S. M., and Hatcher, R. D., Jr., 1980, The Laurel Creek mafic-ultramafic complex, northeast Georgia: Intrusive complex or ophiolite? [abs.]: Geol. Soc. America Abs. with Programs, v. 12, p. 205.

Phillips, N. G., 1980, Water activity changes across an Amphibolite-Granulite facies transition, Broken Hill, Australia: Contr. Mineralogy and Petrology, v. 75, p. 377-386.

Raase, P., 1974, Al and Ti contents of hornblende, indicators of pressure and temperature of regional metamorphism: Contr. Mineralogy and Petrology, v. 45, p. 231-236.

Ramberg, H., 1956, Pegmatites in west Greenland: Geol. Soc. America Bull., v. 67, p. 185-214.

Ramsay, J. G., 1967, Folding and fracturing of rocks: New York, McGraw-Hill, 568 p.

Rankin, D. W., 1970, Stratigraphy and structure of Precambrian rocks on northwestern North Carolina, in Studies of Appalachian geology—central and southern, Fisher, G. W., and others, eds.: New York, Interscience Publishers, p. 227-245.

_____, 1975, The continental margin of eastern North America in the southern Appalachians: The opening and closing of the proto-Atlantic ocean: Am. Jour. Sci., v. 275-A, p. 298-336.

_____, Espenshade, G. H., and Shaw, K. W., 1973, Stratigraphy and structure of the metamorphic belt in northwestern North Carolina and southwestern Virginia: A study from the Blue Ridge across the Brevard fault zone to the Sauratown Mountains anticlinorium: Am. Jour. Sci., v. 273-A, p. 1-40.

Rumble, D., 1973, Fe-Ti oxide minerals from regionally metamorphosed quartzites: Contr. Mineralogy and Petrology, v. 42, p. 181-195.

Russell, B. G., Goudvis, R. G., Domel, G., and Levin, J., 1972, Preliminary report on the analysis of six NIMROC geochemical standard samples: S. Africa, Nat. Inst. Met. Johannesburg, Rep. 1351, 74 p.

Sailor, R. V., and Kuntz, M. A., 1973, Petrofabric and textural evidence for syntectonic recrystallization of the Buck Creek dunite, North Carolina [abs.]: Geol. Soc. America Abs. with Programs, v. 5, p. 791-792.

Sclar, C. B., 1958, The Preston gabbro and the associated metamorphic gneisses, New London County, Connecticut: Connecticut Geol. Nat. History Survey Bull., v. 88, 136 p.

Sen, S. K., 1973, Compositional relations among hornblende and pyroxenes in basic granulites and an application to the origin of garnets: Contr. Mineralogy and Petrology, v. 38, p. 299-306.

Shaw, D. M., 1960, The geochemistry of scapolite: Jour. Petrology, v. 1, p. 218-285.

Shaw, H. F., Wasserburg, G. J., and Albee, A. L., 1981, Sm-Nd, Rb-Sr systematics of mafic complexes and ophiolites of the Appalachians and western U.S. [abs.]: EOS, v. 62, n. 17, p. 409.

Shiraki, K., 1971, Metamorphic basement rocks of Yap islands, western Pacific: Possible oceanic crust beneath an island arc: EPSL, v. 13, p. 167-174.

Spear, F. S., 1976, Ca-amphibole composition as a function of temperature, fluid pressure, and oxygen fugacity in a basaltic system: Carnegie Inst. Wash., Yearb., n. 75, p. 775-779.

_____, 1980, NaSi-CaAl exchange equilibria between plagioclase and amphibole: Contr. Mineralogy and Petrology, v. 72, p. 33-42.

Spry, A., 1969, Metamorphic textures: New York, Pergamon Press Inc., 350 p.

Stevens, R. K., Strong, D. F., and Kean, B. F., 1974, Do some eastern Appalachian ultramafic rocks represent mantle diapirs produced above a subduction zone?: Geology, v. 2, p. 175-178.

Swanson, S. E., 1980, Petrology of the Rich Mountain ultramafic bodies and associated rocks, Watauga County, North Carolina: Southeastern Geology, v. 21, p. 209-225.

Tilley, C. E., 1936a, Paragenesis of kyanite amphibolites: Mineral. Mag., v. 24, p. 555.

_____, 1936b, Paragenesis of kyanite eclogites: Mineral. Mag., v. 24, p. 422.

Tobisch, O. T., 1968, Gneissic amphibolite at Las Palmas, Puerto Rico and its significance in the early history of the greater Antilles island arc: Geol. Soc. America Bull., v. 79, p. 557-574.

Turner, F. J., 1968, Metamorphic petrology: New York, McGraw-Hill.

_____, 1981, Metamorphic petrology, 2nd ed.: New York, McGraw-Hill.

Van De Kamp, P. C., 1969, Origin of amphibolites in the Beartooth Mountains, Wyoming and Montana: New data and interpretation: Geol. Soc. America Bull., v. 80, p. 1127-1136.

Walawender, M. J., 1976, Petrology and emplacement of the Los Pinos pluton, southern California: Can. Jour. Earth Sciences, v. 13, p. 1288-1300.

Walker, K. R., Joplin, G. A., Lovering, J. F., and Green, R., 1960, Metamorphic and metasomatic convergence of basic igneous rocks and lime-magnesia sediments of the Precambrian of northwestern Queensland: Jour. Geol. Soc. Australia, v. 6, p. 149-178.

Waters, A. C., and Campbell, C. D., 1935, Mylonites from the San Andreas fault zone: Am. Jour. Sci., 5th ser., v. 29, p. 473-503.

Wenk, E., and Keller, F., 1969, Isograde in amphibolitserien der Zentralalpen: Schweizerische Mineral. und Petrogr. Mitt., v. 49, p. 157-198.

Wheeler, B. D., 1979, Accuracy in X-ray spectrochemical analysis as related to sample preparation: Symposium on XRF Analysis in Agrochem., Tzinao Institute, Moscow, USSR.

Winkler, H. G., 1979, Petrogenesis of metamorphic rocks, 5th ed.: New York, Springer-Verlag.

Wright, T. L., and Doherty, P. C., 1970, A linear programming and least squares computer method for solving petrologic mixing problems: Geol. Soc. America Bull., v. 81, p. 1995-2008.

APPENDICES

APPENDIX A

X-Ray Fluorescence Methods

Criteria Used for Sample Selection

1. Adequate coverage of the amphibolites within the complex was maintained.

2. The entire continuum of sample variability (in hand sample and in thin section) was covered.

3. Where possible, only those samples which appeared to be *in situ* were chosen.

4. Samples were selected if they were relatively homogeneous on a hand sample scale.

5. Those samples which were badly altered, contained mineralized fractures, or showed significant weathering effects were discarded.

Preparation Procedure

1. Those samples which were chosen for analysis were thoroughly washed with soap and water to remove surface contaminants (sediment buildup, organic material).

2. Samples were then scrubbed with a wire brush to remove as much of the oxidized layer as possible.

3. Samples were then broken into two fist-sized samples, one to be analyzed, the other to be stored.

4. Samples to be analyzed were then scrubbed with a very coarse wire brush to remove oxidation and any remaining oxidized areas were removed with the trim saw.

5. These samples were then cleaned and placed in a jaw crusher which was set at an aperture of 1/4".

6. The crusher was cleaned before and after each use with soap and water and dried thoroughly.

7. Samples were then sieved through -3 phi, -2 phi, and -1 phi sieve sets (sieves were thoroughly cleaned after each use).

8. Anything finer than the -2 phi fraction was discarded. The -3 phi and -2 phi fractions were then examined for inhomogeneous, oxidized, or altered grains. These grains were separated by hand and discarded.

9. Each sample was then placed into a tungsten-carbide rotary mill and ground to a fine powder.

10. Each sample was then split so that a 5 gm sample was obtained. This sample was tared and 100 mg of sodium-stearate were added to facilitate further grinding.

11. Each sample was then ground for 6 mins. in the pulverizer so that each was finer than 200 mesh.

12. Two pressed powder pellets were then made for each sample using a boric acid backing. The exact procedure is described in Wheeler (1979).

Run Conditions

Major element oxides:

Normalization presets:
Condition #1 200 sec.
Condition #2 40 sec.

Concentration Units: %

Analysis condition #1:

Memory size:	1024
Kilovolts:	10.0
Current:	376
Standard preset:	200 sec.
Unknown preset:	100 sec.
Energy range:	2,0-10 keV
Filter:	2,0P
Anode:	0,RH

Regions of interest:

Region Name	Peak Region
NA2O	0.97-1.13
MGO	1.19-1.31
AL2O3	1.42-1.55
SIO2	1.68-1.83
P2O5	1.99-2.03
K2O	3.24-3.42
CAO	3.93-4.12
TIO2	4.45-4.63
CR	5.33-5.58
MNO	5.79-6.03
FE2O3	6.28-6.55

Analysis condition #2:

Memory size:	1024
Kilovolts:	50.0
Current:	176
Standard preset:	40 sec.
Unknown preset:	40 sec.
Energy range:	4,0-40 keV
Filter:	1,SN
Anode:	1,W

Regions of interest:

Region Name	Peak Region	Background Low Region	Background High Region
BA	31.52-32.52	31.16-31.32	32.72-32.92

Trace elements:

Normalization presets:
Condition #1 400 sec.

Concentration units: ppm

Analysis condition #1:

Memory size:	1024
Kilovolts:	50.0
Current:	200
Standard preset:	400 sec.
Unknown preset:	400 sec.
Energy range:	4,0-40 keV
Filter:	1,SN
Anode:	1,W

Regions of interest:

Region Name	Peak Region	Background Low Region	Background High Region
RB	13.20-13.56	12.68-12.80	13.68-13.84
SR	13.92-14.40	13.68-13.84	14.52-14.64
Y	14.80-15.12	14.52-14.64	15.28-15.36
NB	16.44-16.76	16.08-16.20	17.04-17.24
ZR	17.52-17.84	17.04-17.24	18.12-18.32
BA	31.80-32.40	31.20-31.36	32.52-32.64

Matrix correction procedures are those described by Hasler and Kemp (1957). Several calibration curves for standards are shown in Figure A-1.

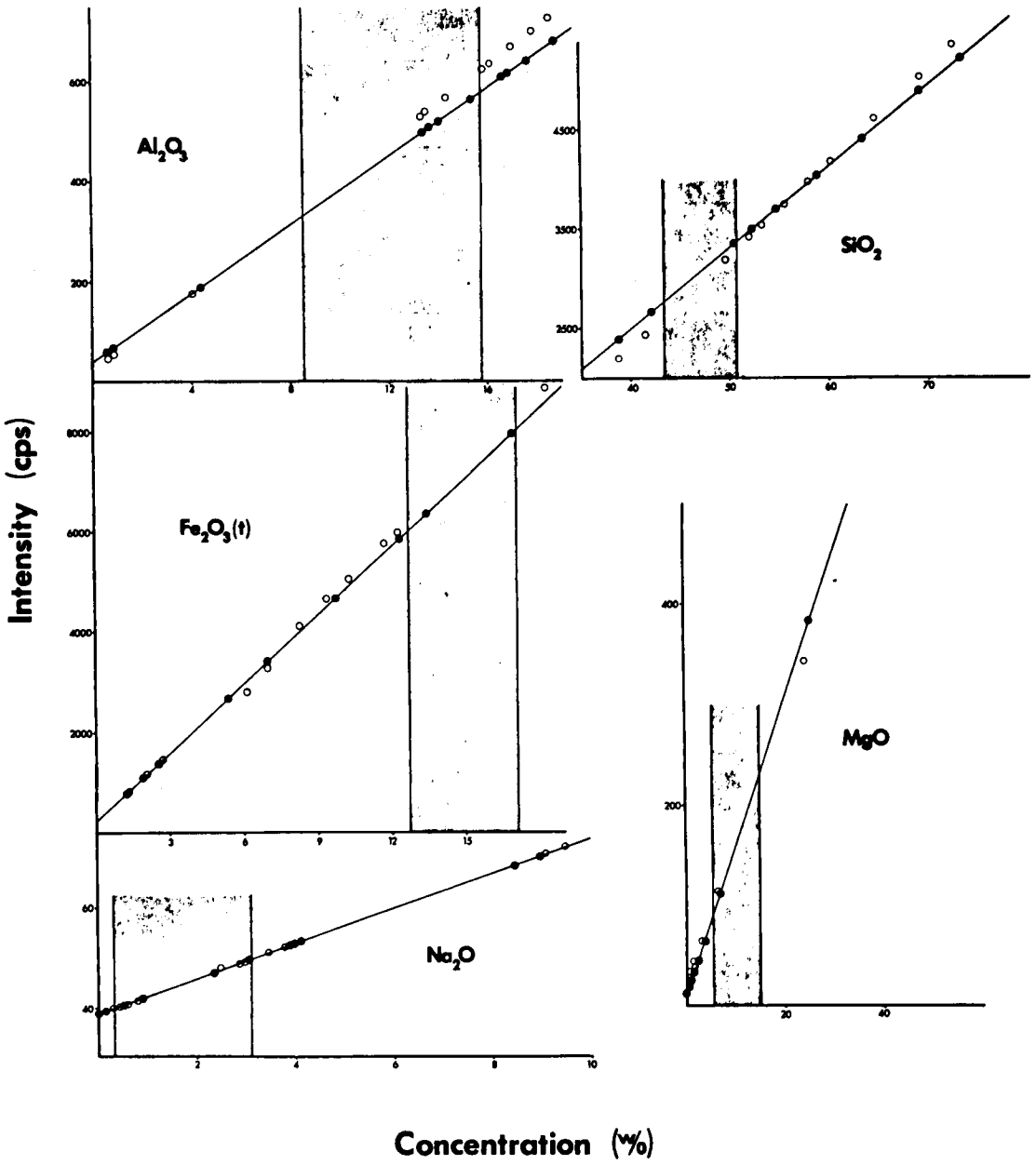

Figure A-1. Selected standard calibration curves for X-ray fluorescence whole-rock analyses. Stippled areas indicate concentration ranges of unknowns. Open circles represent standard compositions before matrix corrections, and closed circles represent standard compositions after corrections. Both compositions have been corrected for background.

Table A-1. Bulk Chemical (XRF) Analyses of Three Standards Run as Unknowns[a]

	Na_2O	MgO	Al_2O_3	SiO_2	P_2O_5	K_2O	CaO	TiO_2	MnO	$Fe_2O_3(t)$[b]
BCR-1	3.1(1)[c]	3.58(2)	13.38(4)	55.0(2)	0.18(1)	1.69(2)	7.05(3)	2.23(1)	0.17(0)	13.38(6)
AGV-1	3.9(2)	1.71(3)	16.9(2)	59.0(3)	0.22(1)	2.93(2)	4.94(1)	1.08(0)	0.09(0)	6.98(8)
SARM4 NIM-N	3.0(3)	7.7(2)	16.8(3)	50.6(2)	0.12(1)	0.21(1)	11.5 (1)	0.20(1)	0.18(0)	10.9 (1)

[a]Mean of three analyses run on separate days.

[b]Total Fe calculated as $Fe_2O_3(t)$.

[c]Units in () represent one standard deviation of replicate analyses in terms of least units cited.

Table A-2. Replicate Analyses of Two Amphibolite Samples[a]

	Na_2O	MgO	Al_2O_3	SiO_2	P_2O_5	K_2O	CaO	TiO_2	MnO	$Fe_2O_3(t)$[b]
3-28	1.7(3)[c]	11.1(5)	13.5(3)	44.0(5)	0.11(1)	0.51(2)	11.4(2)	1.54(2)	0.18(1)	15.6(4)
4-1	2.3(4)	9.1(4)	12.7(2)	47.0(5)	0.13(0)	0.23(1)	13.1(1)	1.50(3)	0.17(1)	15.0(3)

[a]Mean of three analyses run on separate days.

[b]Total Fe calculated as $Fe_2O_3(t)$.

[c]Units in () represent one standard deviation of replicate analyses in terms of least units cited.

APPENDIX B

Table B-1. Average Microprobe Analyses of Hornblendes

	sample 1am8		sample 2-18		sample 4-10		sample 6am34		sample 7-8		sample 8-9		sample 8-15		sample 8-42		sample 12-1	
	A	B	P1-H	SG-H	AB	BI	BB	BC	BA	BE	BD	CC	AA	AB	AA	BB	AA	BB
SiO_2	45.6(3)[b]	45.9(3)	43.0(2)	44.9(4)	44.1(5)	43.48(5)	43.6(4)	43.3(2)	44.4(4)	44.2(5)	43.0(3)	43.9(4)	43.9(3)	43.0(2)	44.4(3)	44.6(1)	45.1(1)	45.0(4)
TiO_2	0.69(2)	0.71(2)	0.62(4)	0.59(5)	0.45(7)	0.54(2)	0.88(3)	0.81(0)	0.94(5)	2.95(2)	0.67(5)	0.52(2)	0.8(1)	0.94(4)	0.47(4)	0.50(3)	1.11(7)	1.07(6)
Al_2O_3	10.7(1)	10.8(1)	12.5(3)	12.9(1)	11.8(3)	12.38(7)	12.9(1)	13.11(4)	12.94(3)	12.48(7)	12.35(6)	11.3(3)	14.2(4)	15.0(3)	13.43(3)	13.1(1)	12.2(1)	12.5(1)
Cr_2O_3	n.d.[c]	n.d.	n.d.	n.d.	n.d.	n.d.	n.d.	n.d.	n.d.	n.d.	n.d.	n.d.	n.d.	n.d.	n.d.	n.d.	n.d.	n.d.
FeO	6.99(9)	8.6(1)	12.8(1)	14.4(3)	12.5(3)	11.63(1)	8.64(9)	7.8(2)	9.2(1)	9.1(2)	10.0(3)	9.1(2)	10.3(2)	11.00(1)	4.4(1)	4.8(1)	11.2(2)	10.2(1)
Fe_2O_3[a]	5.18	3.22	3.58	1.78	1.54	3.23	7.86	8.42	5.53	5.48	5.99	6.75	4.46	4.08	8.35	8.45	4.15	4.22
MnO	0.14(3)	0.14(2)	0.05(2)	0.11(7)	0.23(2)	0.25(1)	0.25(5)	0.29(5)	0.20(2)	0.21(4)	0.22(3)	0.21(8)	0.36(3)	0.30(2)	0.25(0)	0.16(2)	0.21(4)	0.27(4)
MgO	13.7(1)	13.7(1)	10.1(2)	9.9(1)	11.4(1)	11.02(7)	11.3(1)	11.82(6)	12.01(9)	11.9(1)	11.0(1)	11.7(1)	11.1(3)	10.5(1)	13.51(8)	13.63(3)	11.5(2)	11.8(2)
CaO	12.05(9)	12.00(7)	11.90(3)	11.98(4)	11.7(1)	11.63(7)	11.4(1)	11.6(1)	11.90(7)	11.74(2)	11.49(5)	11.59(7)	11.71(9)	11.7(1)	11.4(1)	11.6(1)	11.9(1)	11.92(7)
Na_2O	1.22(5)	1.30(7)	1.34(4)	1.32(6)	2.0(2)	2.00(0)	1.79(8)	1.86(7)	1.59(2)	1.56(2)	1.60(5)	1.49(5)	1.75(9)	1.87(9)	1.53(1)	1.48(5)	1.75(9)	1.61(9)
K_2O	0.47(4)	0.94(3)	0.63(5)	0.69(2)	0.55(0)	0.55(1)	0.32(0)	0.31(2)	0.21(1)	0.19(0)	0.63(2)	0.57(4)	0.6(1)	0.71(5)	0.43(1)	0.45(2)	0.26(2)	0.25(2)
Total	96.95	97.57	96.70	98.69	96.43	96.71	99.12	99.47	98.97	97.95	97.06	97.22	99.49	99.32	98.25	98.88	99.72	99.06
Formula Basis (oxygens)	23																	
Si	6.641	6.675	6.450	6.577	6.588	6.474	6.317	6.247	6.399	6.442	6.383	6.482	6.332	6.232	6.352	6.365	6.498	6.492
Ti	0.075	0.077	0.070	0.065	0.050	0.060	0.096	0.088	0.102	0.104	0.075	0.058	0.095	0.102	0.051	0.054	0.120	0.116
Al^{IV}	1.390	1.330	1.550	1.420	1.200	1.530	1.680	1.750	1.600	1.560	1.620	1.520	1.670	1.770	1.650	1.640	1.500	1.510
Al^{VI}	0.490	0.520	0.660	0.810	0.670	0.640	0.520	0.480	0.600	0.580	0.540	0.460	0.75	0.810	0.610	0.560	0.580	0.620
Cr	n.d.	n.d.	n.d.	n.d.	n.d.	n.d.	n.d.	n.d.	n.d.	n.d.	n.d.	n.d.	n.d.	n.d.	n.d.	n.d.	n.d.	n.d.
Fe^{2+}	0.850	1.054	1.613	1.766	1.558	1.448	1.045	0.951	1.113	1.114	1.243	1.124	1.242	1.331	0.527	0.575	1.348	1.238
Fe^{3+}	0.567	0.352	0.403	0.196	0.173	0.362	0.856	0.914	0.599	0.600	0.669	0.750	0.483	0.445	0.899	0.903	0.449	0.457
Mn	0.017	0.017	0.006	0.014	0.029	0.032	0.031	0.035	0.024	0.026	0.028	0.026	0.044	0.037	0.030	0.019	0.035	0.033
Mg	2.980	2.973	2.256	2.162	2.533	2.446	2.444	2.540	2.579	2.583	2.448	2.574	2.390	2.281	2.880	2.894	2.467	2.538
Ca	1.877	1.866	1.909	1.878	1.872	1.855	1.778	1.797	1.837	1.830	1.827	1.833	1.806	1.818	1.756	1.772	1.846	1.840
Na	0.344	0.366	0.389	0.375	0.578	0.577	0.502	0.520	0.444	0.440	0.460	0.426	0.488	0.525	0.424	0.409	0.488	0.450
K	0.087	0.174	0.120	0.129	0.105	0.104	0.059	0.057	0.039	0.035	0.119	0.107	0.112	0.131	0.078	0.082	0.048	0.046

[a] Fe_2O_3 calculated.

[b] Units in () represent one standard deviation of replicate analyses in terms of least units cited.

[c] n.d. = not detected; less than 0.03%.

Table B-2. Average Microprobe Analyses of Plagioclases

Sample:	2-18	4-10		6am34		8-9		8-15		8-42		12-1	
	Hb1-P1	AF	BH	BD	BE	AC	BG	AC	AF	AD	AF	AE	AF
SiO_2	60.1(3)[a]	61.9(2)	62.4(2)	54.9(5)	55.7(2)	62.1(2)	61.5(4)	63.6(3)	60.4(2)	55.6(4)	55.0(2)	49.8(2)	50.1(3)
Al_2O_3	25.2(2)	25.1(2)	24.3(2)	28.9(1)	28.33(4)	24.4(2)	24.5(1)	23.6(1)	23.9(1)	28.4(1)	28.6(1)	32.26(7)	32.6(1)
CaO	6.4(2)	5.8(4)	5.2(4)	10.88(6)	10.86(7)	5.5(1)	5.7(1)	4.8(2)	4.8(2)	10.48(8)	10.7(1)	14.98(6)	14.9(1)
Na_2O	7.8(3)	8.0(2)	8.2(2)	5.42(7)	5.26(5)	8.4(1)	8.4(2)	9.0(3)	8.9(3)	5.6(1)	5.4(1)	3.1(1)	3.1(2)
K_2O	0.07(1)	0.07(2)	0.07(1)	n.d.[b]	n.d.	0.07(0)	0.06(2)	n.d.	n.d.	n.d.	n.d.	n.d.	n.d.
Total	99.77	100.96	100.38	100.16	100.20	100.55	100.27	101.2	98.11	100.27	99.86	100.16	100.71
Formula Basis (oxygens)	8												
Si	2.681	2.717	2.750	2.468	2.500	2.736	2.722	2.780	2.729	2.496	2.481	2.267	2.264
Al	1.325	1.298	1.264	1.531	1.497	1.268	1.278	1.218	1.274	1.503	1.519	1.729	1.738
Ca	0.309	0.273	0.247	0.523	0.521	0.260	0.269	0.224	0.232	0.502	0.515	0.729	0.723
Na	0.675	0.685	0.703	0.472	0.457	0.718	0.724	0.765	0.779	0.488	0.474	0.273	0.275
K	0.004	0.003	0.003	n.d.	n.d.	0.002	0.002	n.d.	n.d.	n.d.	n.d.	n.d.	n.d.

[a] Units in () represent one standard deviation of replicate analyses in terms of least units cited.

[b] n.d. = not detected; less than 0.03%.

Table B-3. Average Microprobe Analyses of Garnet, Epidote, and Clinopyroxene

Sample:	2-18			7-8		4-10	6am34	12-1		
	Gar (avg.)[b]	Gar (core and rim)	Gar (int.)	Epid	Epid	Epid	Cpx	Cpx	Cpx	Cpx
SiO_2	37.5(3)[c]	37.4(5)	37.3(5)	39.0(1)	37.2(4)	37.7(1)	49.9(1)	51.0(1)	50.0(1)	50.7(1)
TiO_2	--	--	--	n.d.	0.11(4)	0.12(2)	0.29(2)	0.33(3)	0.31(2)	0.31(4)
Al_2O_3	21.2(2)	21.6(3)	21.7(2)	26.7(1)	28.11(7)	26.5(5)	4.9(1)	4.4(2)	4.4(2)	4.0(3)
Cr_2O_3	n.d.[d]	n.d.	n.d.	n.d.	n.d.	n.d.	n.d.	n.d.	n.d.	n.d.
FeO[a]	24 (1)	21.6(1)	26.7(2)	8.0(3)	6.9(2)	7.2(1)	9.3(1)	9.2(4)	9.6(1)	9.5(4)
MnO	2.8(3)	3.1(5)	2.6(4)	0.20(7)	0.18(1)	0.11(2)	0.25(3)	0.27(4)	0.25(2)	0.24(4)
MgO	2.0(1)	1.4(2)	2.4(2)	0.09(0)	0.11(1)	0.09(1)	12.2(1)	12.6(1)	12.3(1)	12.7(1)
CaO	11 (1)	14.1(1)	9.2(1)	23.77(1)	23.30(6)	23.4(1)	23.1(2)	21.0(5)	20.6(1)	20.9(2)
Na_2O	--	--	--	n.d.	0.07(3)	n.d.	0.70(4)	0.66(5)	0.70(7)	0.58(5)
K_2O	--	--	--	n.d.	n.d.	n.d.	n.d.	n.d.	n.d.	n.d.
Total	99.61	99.44	100.11	97.82	96.09	95.39	100.86	99.70	98.41	99.06
Formula Basis (oxygens)	12	12	12	25	25	25	6	6	6	6
Si	2.987	2.972	2.961	6.180	5.983	6.120	1.862	1.909	1.900	1.913
Ti	--	--	--	n.d.	0.009	0.014	0.007	0.008	0.009	0.007
Al	1.993	2.020	2.032	4.988	5.327	5.070	0.217	0.194	0.198	0.178
Cr	n.d.	n.d.	n.d.	n.d.	n.d.	n.d.	n.d.	n.d.	n.d.	n.d.
Fe^{2+}	1.654	1.431	1.769	1.060	0.934	0.014	0.290	0.290	0.306	0.299
Mn	0.189	0.209	0.174	0.023	0.023	0.014	0.007	0.007	0.007	0.006
Mg	0.238	0.169	0.293	0.018	0.023	0.018	0.678	0.705	0.701	0.711
Ca	0.968	1.203	0.784	4.035	4.011	4.075	0.925	0.841	0.838	0.843
Na	--	--	--	n.d.	0.018	n.d.	0.050	0.047	0.050	0.042
K	--	--	--	n.d.	n.d.	n.d.	n.d.	n.d.	n.d.	n.d.

[a] All Fe calculated as FeO.

[b] Average of 32 analyses from a traverse across single garnet; average analysis of 7 core and rim compositions and 4 intermediate compositions are also reported for the same garnet.

[c] Units in () represent one standard deviation of replicate analyses in terms of least units cited.

[d] n.d. = not detectable; less than 0.03%.

VITA

Matthew Stuart McElhaney was born in Fredericksburg, Virginia on July 6, 1957. He graduated from Wilton Senior High School, Wilton, Connecticut in June of 1975. He attended the United States Merchant Marine Academy from July 1975 until June 1976, where he studied Engineering. He then transferred to the College of William and Mary, where he received a Bachelor of Science degree in Geology in December 1979. In the winter of 1980 he accepted a teaching assistantship at The University of Tennessee, Knoxville. He received a Master of Science degree in Geology in December 1981.

The author is a member of Sigma Gamma Epsilon (a geology honorary society), the Geological Society of America, and the Mineralogical Society of America. Mr. McElhaney has accepted a position as an Exploration Geologist with Shell Oil Company in Houston, Texas.

He is married to the former Sharla Kay Jones of Grafton, Virginia.